1993

Growth and characterization of polysilicon films deposited by reactive plasma beam epitaxy

Behnam Moradi
Iowa State University

INFORMATION TO USERS

This manuscript has been reproduced from the microfilm master. UMI films the text directly from the original or copy submitted. Thus, some thesis and dissertation copies are in typewriter face, while others may be from any type of computer printer.

The quality of this reproduction is dependent upon the quality of the copy submitted. Broken or indistinct print, colored or poor quality illustrations and photographs, print bleedthrough, substandard margins, and improper alignment can adversely affect reproduction.

In the unlikely event that the author did not send UMI a complete manuscript and there are missing pages, these will be noted. Also, if unauthorized copyright material had to be removed, a note will indicate the deletion.

Oversize materials (e.g., maps, drawings, charts) are reproduced by sectioning the original, beginning at the upper left-hand corner and continuing from left to right in equal sections with small overlaps. Each original is also photographed in one exposure and is included in reduced form at the back of the book.

Photographs included in the original manuscript have been reproduced xerographically in this copy. Higher quality 6" x 9" black and white photographic prints are available for any photographs or illustrations appearing in this copy for an additional charge. Contact UMI directly to order.

U·M·I

University Microfilms International
A Bell & Howell Information Company
300 North Zeeb Road, Ann Arbor, MI 48106-1346 USA
313/761-4700 800/521-0600

Order Number 9321198

Growth and characterization of polysilicon films deposited by reactive plasma beam epitaxy

Moradi, Behnam, Ph.D.

Iowa State University, 1993

U·M·I
300 N. Zeeb Rd.
Ann Arbor, MI 48106

Growth and characterization of polysilicon films deposited by reactive plasma beam epitaxy

By

Behnam Moradi

A Dissertation Submitted to the
Graduate Faculty in Partial Fulfillment of
the Requirement for the Degree of
DOCTOR OF PHILOSOPHY

Department: Electrical Engineering and Computer Engineering
Major: Electrical Engineering (Microelectronics)

Approved:

Signature was redacted for privacy.

In Charge of Major Work

Signature was redacted for privacy.

For the Major Department

Signature was redacted for privacy.

For the Graduate College

Iowa State University
Ames, Iowa

1993

TABLE OF CONTENTS

ABSTRACT

Polycrystalline silicon was deposited at low temperatures (400-550 ^{o}C) by using a new technique, reactive plasma beam epitaxy. The technique consists of using an intense flux of hydrogen radicals, generated by an electron cyclotron resonance (ECR) source to promote nucleation and crystallinity at low temperatures. The film structure could be smoothly changed from polysilicon to amorphous by changing the flux of incoming H radicals on the surface of the sample. The flux of hydrogen radicals can be controlled by changing the deposition pressure, with lower pressures leading to a higher H radical flux and greater degree of crystallinity. The effect of H radicals on the growth of polysilicon films was studied by using two different plasma characterizations techniques, namely Langmuir probe and optical emission spectroscopy. Both n and p type films were deposited by using a phosphine and diborane mixture in hydrogen. The growth rate is found to be independent of the doping or of the deposition temperature. The crystalline nature of the films was verified by using Raman spectroscopy. The crystallographic orientations of the films were examined by x-ray diffraction. The grain size of the polysilicon films was estimated by using the full width at half maximum of x-ray diffraction spectra, and were of the order of 200Å. There was no significant change in either the grain size or the orientation of the films as the deposition temperature was increased from 400 to 550 ^{o}C. Surface morphology of the films was studied by using scanning electron microscope and ultraviolet reflectance measurements. The electronic properties of the polysilicon films were examined by conductivity, activation energy and Hall mobility measurements. The results of these

characterization techniques indicate that the as deposited films are slightly n type, and they have high mobilities (40 $cm^2/v.s$).

I. INTRODUCTION

A. Background

Polycrystalline silicon (polysilicon) is an important electronic material and has a variety of applications in integrated circuit technology. From a structural point of view, polysilicon is neither like single crystalline silicon with a perfect periodic structure nor it is completely disordered like amorphous solids. Small crystalline regions, grains, still exist but separated from each other by grain boundaries. This unique structure has made polysilicon a very useful material and a handy solution to many technological problems in integrated circuits.

It is well known that the development of the high density metal oxide semiconductor (MOS) integrated circuits has resulted in the production of the complex logic circuits and high density memory chips. The key in fabrication of such high density integrated circuits is the use of polysilicon films as the gate electrode of the MOS devices, which allows the realization of the self aligned process. (i.e. using the polysilicon as a mask to define the source and the drain of an MOS device). This is one of the most fundamental developments in the field of MOS technology, which has improved electrical characteristics as well as packing density of the integrated circuits. In addition, the polysilicon gate provides a more compatible threshold voltage with the voltages used to bias integrated circuits [1]. The use of polysilicon films is not limited to the gate electrode of MOS devices. Lightly doped polysilicon films are frequently used as high value resistors in static memories. Heavily doped polysilicon films are usually used as interconnections in the integrated circuits [2].

The compatibility of polysilicon with standard silicon processing has allowed more complex fabrication sequences. For example, phosphorus doped silicon dioxide (phosphosilicate glass or PGS) can be deposited over a polysilicon layer and heated until its viscosity decreases and it flows. This decreases the angle of the steps which aluminum needs to cover for the contact windows. The processing compatibility of polysilicon has been also used in the fabrication of dynamic random access memories (DRAM), where one layer of the polysilicon serves as the gate of the access transistor and one as the counter-electrode of the storage capacitor.

In bipolar integrated circuits, a polysilicon layer between the base region and the base contact reduces the parasitic capacitance. Polysilicon has been also widely used to self-align the emitter region to the base. This significantly improves the packing density. In all integrated circuits, aluminum spiking has been minimized by using a layer of polysilicon between the silicon substrate and aluminum contacts. Other applications of polysilicon films are diffusion source for shallow junctions, low cost large area solar cells and thin film transistors [1]. In all of these applications, the device characteristics highly depend on the deposition techniques.

In early years of polysilicon development, (1963-1970), polysilicon films were deposited by physical vapor deposition. Poor coverage, unwanted impurities, thickness variation and low productivity prevented wide spread use of this technique [3]. In early stages of manufacturing (1970-1976) chemical vapor deposition in horizontal atmospheric pressure reactors, which was a well developed technique for bipolar integrated circuits, was found to be a good replacement for the physical vapor deposition. This reactor offers large grain

size films at 900 ^{o}C and smaller grain size at 650 ^{o}C[1]. The Low pressure chemical vapor (LPCVD) deposition system which was introduced in 1976 has been widely used in the production of high volume integrated circuits. Since LPCVD is based on the pyrolysis reaction, it is very sensitive to the deposition temperature. Analysis of LPCVD parameters, structure, properties and applications of LPCVD polysilicon films have been extensively studied and reviewed by T. Kamin [1], W. Kern, [4] and G. Harbeke [5].

Although LPCVD has been widely used in the production of the polysilicon for integrated circuits, it suffers from several problems including [6]:

1. Sensitivity of the film thickness to the deposition temperature.
2. Severe reduction in thickness uniformity and deposition rate by introducing dopants such as phosphorus and arsenic.
3. High deposition temperature which is not suitable for the sub-micron technology.

The capability of incorporating a large number of impurities during the deposition of polysilicon is particularly important in applications such as gate electrodes of MOS devices.

In recent years low temperature deposition has stimulated a great deal of interest in studying and developing new methods to replace conventional CVD systems. Much attention has been attracted to plasma-enhanced chemical vapor deposition (PECVD). PECVD which was originally developed for the deposition of dielectric films has been found to be the most promising technique because it offers advantages such as:

1. Less sensitivity to deposition temperature.
2. Higher growth rate.

3. Lower deposition temperature.

4. Capability of introducing high doping concentration without affecting the growth rate.

Glow discharge, which is extensively used in the deposition of amorphous silicon films, was among the first PECVD methods utilized for the growth of polysilicon films. In 1979 F. Morin and his coworkers [7] reported the deposition of polysilicon films by using glow discharge. They deposited undoped films with an argon plasma at temperatures ranging from 250 to 650 ^{o}C in a reaction chamber which was made of a quartz tube and was inserted in a horizontal furnace. They evaluated the crystalline quality of the films by using the reflection high-energy electron diffraction (RHEED) technique. Based on the RHEED analysis they reported that films deposited above 500 ^{o}C were polysilicon with the (110) preferred orientation. They did not report on the other structural properties or electrical and optical characteristics of the deposited films. Although sharp rings from RHEED analysis support the fact that some degree of crystallinity is present in the deposited films, it is not a conclusive method for determining the quality of the polysilicon films.

In 1980, S. Veprek [8] reported the deposition of polysilicon films at temperatures lower than 400 ^{o}C by chemical transport in a hydrogen plasma. They characterized the grown films by the means of x-ray diffraction as well as Raman spectroscopy. The Raman spectra they reported are more characteristic of microcrystalline silicon than polysilicon with sharp peaks at 516-519 cm^{-1} and broad peaks at 480 cm^{-1}. Moreover, they did not report the electrical properties of the deposited films except a conductivity of 10^{-6} S/cm.

In 1982 T. Kamin and K. L. Chiang [9] deposited polysilicon films by

using a PECVD reactor in which they could process more than one hundred wafers simultaneously. They grew films at temperatures ranging from 525 to 750 ^{o}C with argon as the plasma gas and dichlorosilane as the process gas. The results of x-ray, transmission electron microscopy (TEM) and reflectance measurements that they performed on the deposited films indicated that the films deposited at or below 600 ^{o}C were amorphous while those deposited at 625 ^{o}C and above were polysilicon with a poorly defined structure.

In 1986, J. J. Hajjar et. al [10] tried the deposition of polysilicon films by decomposition of silane at temperatures between 500 to 800 ^{o}C at a very low pressure of 4mT. Based on the x-ray differaction results, as well as other measurements they concluded that films deposited with the assistance of a plasma were amorphous at temperatures of 650 ^{o}C and below. In their more recent papers [11] they report on polysilicon films deposited by PECVD from AsH_3/SiH_4 and B_2H_6/SiH_4 mixtures and the film properties were the same as reported in their previous work.

Other workers have investigated the possibility of other PECVD based techniques such as reactive ion beam techniques and remote plasma CVD systems. H. Yamada et. al [12] have studied the possibility of the deposition of polysilicon by using the reactive ion beam method. Their reactive ion beam system consists of an ECR source, a deposition chamber and a substrate exchange chamber. They deposited polysilicon films by using an ion-assisted crystallization technique. In this method, amorphous silicon was first deposited on silicon dioxide substrates at temperatures between 100-150 ^{o}C. Crystallization was then achieved by bombarding the substrate with a flux of hydrogen radicals at 600 ^{o}C.

G. Lucovsky's group [13] at North Carolina State University has extensively studied the deposition of microcrystalline films as well as dielectric materials by using remote PECVD. Unlike other deposition techniques, in the remote PECVD method the process gasses are not directly subjected to the plasma excitation. In this method, silane and the dopant atom source gases are remotely excited by the species transported out of the noble gas plasma, usually helium. Other techniques which have also attracted attention in recent years are rapid thermal annealing, rapid thermal processing and laser annealing [14].

Overall, the polysilicon deposition techniques that are cited in the literature can be divided into two categories. The first involves high temperatures growth i.e. 650 to 1000 ^{o}C. The second relies either on high temperature post deposition annealing or grain boundary passivation by hydrogen plasma. While the first method has a difficulty in fulfilling the requirement of submicon device process for very large scale integration (VLSI) and ultra large scale integration (ULSI), the second method suffers from non uniformity of hydrogen diffusion at the grain boundaries and the small grain size of amorphous silicon.

B. Scope

The purpose of this research was to grow and characterize high quality polysilicon films at low temperatures by using in-situ grain boundary annealing. Such a study is important because the future of VLSI and ULSI circuits requires the development of new deposition techniques that can deposit high quality films at low temperatures. While most of the investigators have identified the

substrate temperature as the main parameter that causes the transition from amorphous to polysilicon, we have studied the importance of the hydrogen flux on the film formation and phase transition.

The deposition system used in this research investigation is an electron cyclotron resonance plasma deposition system., which we refer to as reactive plasma beam epitaxy (RPBE). By using RPBE system we can alter the film structure by controlling the flux of incoming hydrogen radicals and consequently deposit amorphous, microcrystalline and polycrystalline silicon at the same temperature but different pressure.

Intrinsic and doped polysilicon films are deposited on different substrates at different temperatures, pressures, powers and doping concentrations. Influence of the plasma species on the growth mechanism is investigated by two different plasma diagnostic techniques, namely Langmuir probe and optical emission spectroscopy. Crystallinity and the grain size of the samples are examined by Raman spectroscopy and x-ray diffraction. Thickness, surface roughness, band gap and index of refraction are calculated by the means of optical measurements. Scanning electron microscopy technique is used to investigate the surface morphology. Depth profile of the phosphorus dopants as well as other impurities are examined by secondary ion mass spectroscopy. Electronic properties of the deposited films are studied by conductivity, Hall mobility and activation energy measurements. Inter-grain tunneling is investigated by measuring Hall mobility vs. temperature. The carrier transport mechanism in the films is examined by studying of the behavior of conductivity as a function of temperature.

II. PHYSICS OF POLYSILICON

The physics of polysilicon is largely the physics of grain boundaries. Defects resulting from the incomplete atomic bonding causes the carriers to be trapped in the grain boundary regions. This has a significant effect on the performance of polysilicon devices. As a result, the electrical properties including mobility, diffusion length and life time of polysilicon films are much lower than crystalline silicon. There are two schools of thought concerning the effect of grain boundaries on the transport properties of the polysilicon films, the segregation theory and the trapping models [15].

A. Segregation Theory

Segregation theory, which was first reported by Cohwer and Sedgwick [16], interprets the grain boundaries as a sink for impurity atoms. According to this model, the impurity atoms tend to segregate at the grain boundary, where they become electrically inactive. Consequently, the amount of impurities in the crystalline regions is reduced, which results in a lower carrier concentration than for a uniformly distributed doping concentration. This means that the carrier concentration does not approach the doping concentration until the boundaries are saturated with impurity atoms. The basic limitation of segregation theory is that it does not explain either the temperature dependence of the resistivity, or the minimum Hall mobility at intermediate carrier concentrations.

B. Trapping Model

The second model postulates that the higher resistivity of polysilicon films at low doping concentrations compared to single crystal silicon is due to the trapping of active carriers at the lower energy position of the grain boundaries [17]. This group reasons that since there are many disordered atoms at the boundaries, there are a large number of trapping states. These states are capable of trapping the carriers and immobilizing them. Assuming that the defects in the grain boundaries are initially neutral with a density of N_T, upon trapping the dopant atoms they will produce a charged grain boundary. Since charge neutrality must hold, an oppositely charged region will be a depleted in the grain regions. From Poisson's equation it is possible to show that depleted charge region causes a curvature in the energy band and hence creates a potential barrier which impedes the movement of the remaining free carriers. This is schematically shown in Figure 2.1 The height of the barrier can be calculated from the knowledge of the doping density and the Poisson's equation.

$$\frac{d^2V}{dX^2} = \frac{qN}{\varepsilon} \tag{2.1}$$

where q is the electric charge, N is the doping density and ε is the permitivity of the silicon. Solving this differential equation with proper boundary conditions results in,

$$V_B = \frac{qNX^2}{2\varepsilon} \tag{2.2}$$

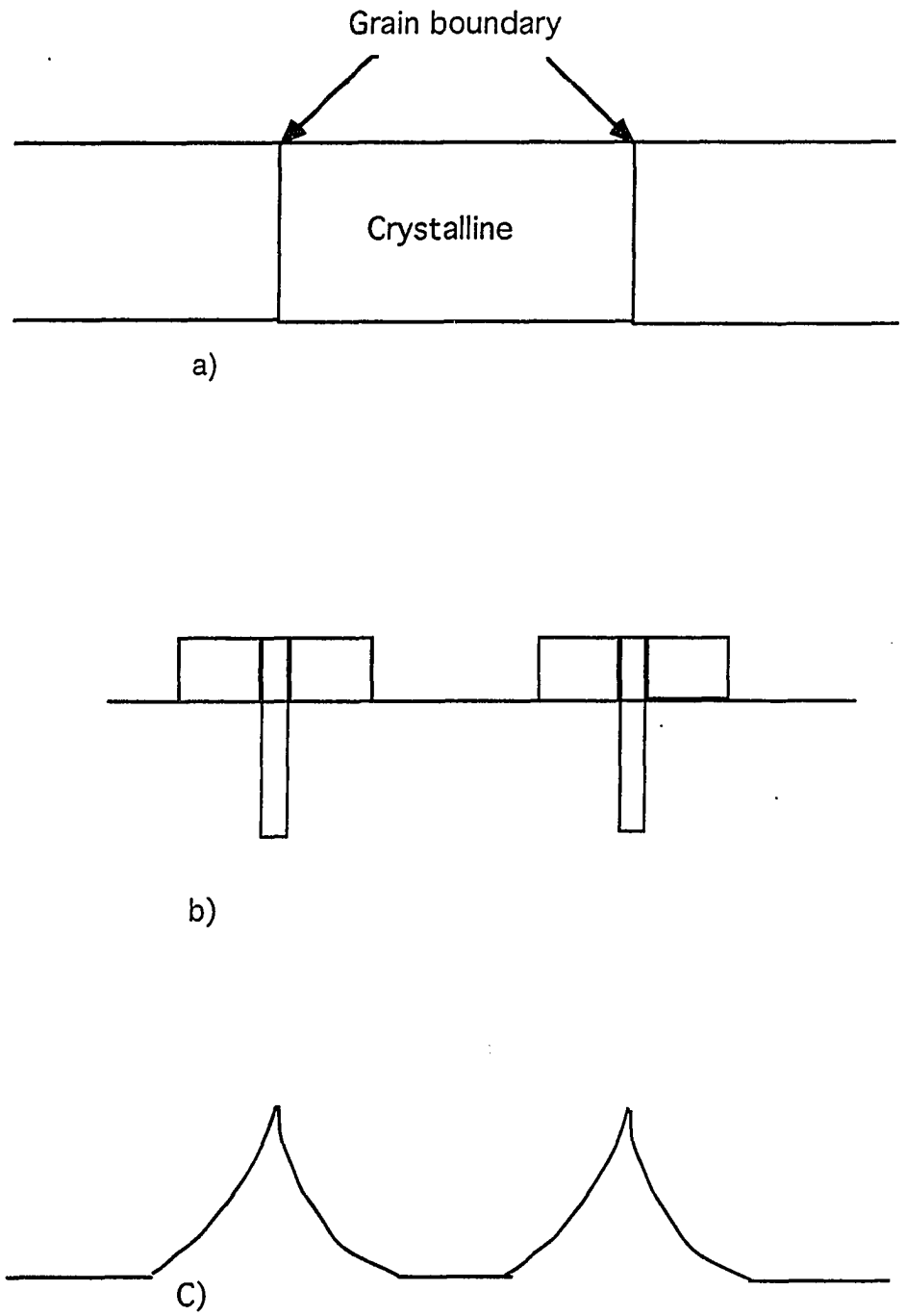

Figure 2.1 Energy band diagram of polysilicon a) crystal structure of poly silicon, b) charge distribution, c) barrier height

This shows a very strong dependence of the barrier height on the doping concentration. For a low doping density, when the product of the doping concentration and the grain size (L), N*L (per unit area), is less than trap density ,N_T, all the carriers will be trapped in the grain boundary. This causes the depletion region surrounding the grain boundary to extend through the grain region and hence eliminate the neutral region. Moreover, the low doping concentration means less curvature of the energy band and consequently lower barrier height. In this case, free carriers, if present, can easily overcome the barrier and move to the next grain. When the grain is totally depleted, then X can be replaced by L/2 and the barrier height will be [15]:

$$V_B = \frac{qNL^2}{8\varepsilon} \tag{2.3}$$

As the doping concentration increases more carriers will be trapped in the grain boundary which results in larger barrier height. However, there is a critical doping density at which [1]:

$$N_T/L = N^* \tag{2.4}$$

where N* is denoted as critical density. Once the doping density has reached its critical value the number of the trapped carriers remains constant and from charge neutrality,

$$X = N_T/2N \tag{2.5}$$

Substituting this value in equation (2.1) results in a barrier height of

$$V_B = \frac{qN_T^2}{8\varepsilon N} \tag{2.6}$$

Equation (2.6) shows that a further increase in doping concentration will result in a lower barrier height. In summary, the barrier height first increases and then starts to decrease. This behavior of the barrier height has a profound impact on the electrical transport in polysilicon.

By combining the trapping model with the thermionic emission mechanism, Seto [15] developed a comprehensive model of transport in polysilicon films. Although this model is capable of explaining most of the electrical properties of polysilicon films, it is only valid for a δ-shape distribution of states and the case of completely filled trap states. G. Baccarini and R. Rico [18] modified Seto's theory by including both the case of monovalent trapping states and that of a continuous distribution of states within the band gap.

C. I-V Characteristics

Understanding of current transport in polysilicon is important because proper device design requires models that can predict and explain the effects of the parameters such as doping concentration, mobility, type of dopants and the operating temperature on the device characteristics. A pioneering work on the modeling of conduction in polysilicon was reported by T. Kamin [17]. He attributed the lower Hall mobility as well as lower conductivity of polysilicon films to the presence of the barrier. Seto [15] quantified the barrier height over a wide range of the carrier concentration and concluded that the thermionic

emission is the dominant conduction mechanism in polysilicon films. C-C Lu, et. al [19] considered the polysilicon films as a material with two distinct resistivities; one due to the grain boundary, and the other resulting from the grain regions. Based on this assumption, they developed a model which entails two modes of conduction. One involves the conduction in the crystal region where the current is limited by the phonon scattering, The other mode of conduction takes place in the depletion region where carriers must either tunnel or overcome the barrier height. In all of these models, an artificial factor was needed to fit the experimental data to the theory. To eliminate this factor, M. Mandurah et. al [2] proposed that a scattering factor must be included in the conduction mechanism of polysilicon films. This factor was attributed to the amorphous nature of the grain boundaries. Dae M Kim et. al [20] have treated the grain boundary as an amorphous semiconductor in equilibrium contact with a crystalline semiconductor. Based on this assumption, they have shown that current in polysilicon films can be described in terms of drift and diffusion.

D. Derivation of I-V Characteristics

By using the WKB transmission approximation and Maxwell-Boltzman statistics, it is possible to derive a simplified version of the J-V expression of polysilicon films. In this derivation the grain boundary width is considered to be negligible compared to the grain size. Assuming that the barrier height consists of two Schottky barriers and applying the abrupt depletion approximation, the space charge potential barrier is given as,

$$V(x) = \frac{qNx^2}{2\varepsilon} \tag{2.7}$$

The one dimensional time independent WKB transmission probability for a barrier is [21],

$$\tau(E) = \exp\left(\frac{-4\pi}{h}\right)\int_{x1}^{w}\{2m^*[qV(x)-E]\}^{1/2}dx \qquad (2.8)$$

where m* is effective mass, E is energy and X_1 and w are shown in Figure 2.2. Substituting (2.7) into (2.8), τ(E=0) can be written as:

$$\tau(E=0) = \exp\left(-\frac{E_b}{E_{00}}\right) \qquad (2.9)$$

where E_{oo} is defined as

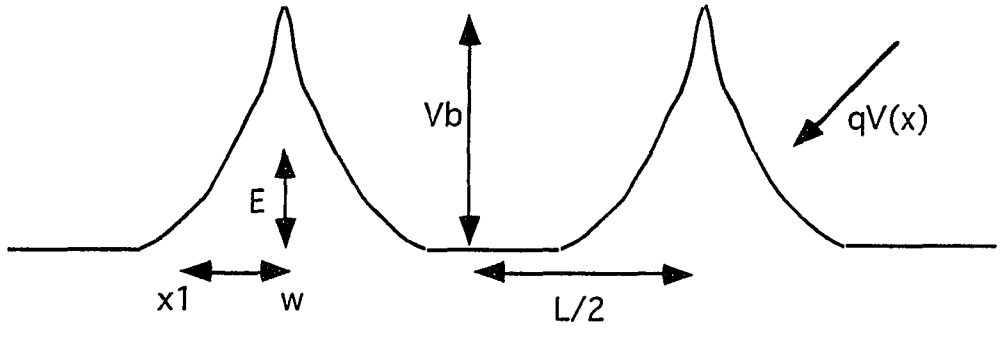

Figure 2.2 Potential Energy vs. distance

$$E_{00} = \frac{qh}{8\pi}\left[\frac{N}{m\varepsilon}\right]^{1/2} \tag{2.10}$$

Here h is Plank's constant. It should be noted that E_{00} is smaller by a factor of two compared to the value reported for the Schottky barrier. If we define

$$U = \frac{qNX^2}{2\varepsilon} - E \tag{2.11}$$

and change the integral limit from distance to energy, then $\tau(E)$ can written as

$$\tau(E) = \exp\left(-\frac{E_b y(\alpha)}{E_{00}}\right) \tag{2.12}$$

and $y(\alpha)$ is defined as

$$y(\alpha) = (1-\alpha)^{1/2} - \alpha \ln\left[\frac{1+(1-\alpha)^{1/2}}{\sqrt{\alpha}}\right] \tag{2.13}$$

where $\alpha = E_b/E$. The net current resulting from applying a small voltage is given by [21],

$$J = J_{l-R} - J_{R-l} = \frac{A^* T}{K}\left[\int_0^\infty \tau(E) f_l dE - \int_0^\infty \tau(E) f_R dE\right] \tag{2.14}$$

where A* is Richardson constant defined as [22],

$$A^* = \frac{4\pi q m^* K^2}{h^3}$$

where m* is the effective mass of silicon. If the voltage across the space charge region, V_S, and the voltage across the grain boundary are equally divided on each side of the junction then,

$$f_L = \exp\left[\left(-E + E_f + \frac{qV_s}{2} + \frac{qV_{GB}}{2}\right)\right] \tag{2.15}$$

$$f_R = \exp\left[\left(-E + E_f - \frac{qV_s}{2} - \frac{qV_{GB}}{2}\right)\right] \tag{2.16}$$

$$J = \frac{A^* T}{K}\left(\int_0^E f\tau(E) + \int_E^{E_b} f\tau(E) + \int_{E_b}^{\infty} f\tau(E)\right)dE \tag{2.17}$$

Substituting (2.15) and (2.16) into (2.17),

$$J = C\left(\int_0^E \exp(-\frac{E}{KT})\tau(E) + \int_E^{E_b} \exp(-\frac{E}{KT})\tau(E) + \int_{E_b}^{\infty} \exp(-\frac{E}{KT})\tau(E)\right)dE \tag{2.18}$$

where

$$C = \frac{2A^{*}T}{K}\exp(\frac{E_f}{KT})Sinh\left(\frac{q(V_{GB}+V_S)}{2KT}\right) \qquad (2.19)$$

The first integral describes thermionic field emission through the depletion layer and the grain boundaries, while the second integral describes the thermionic field emission through the grain boundaries. The third integral is the expression for thermionic emission. Since the probability of tunneling through both the grain and the grain boundaries is very small, the first term can be neglected.

According to (2.18), when carriers have sufficient energy to surmount the potential barrier in the depletion layer of the grains and the grain boundary barrier, then the current transport is pure thermionic emission. On the other hand, inter-grain tunneling is the dominant process, when the carriers have sufficient energy to tunnel through the grain boundaries. When thermionic emission is the dominant process, the conductivity and the mobility can be derived by using equation(2.18) and (2.20a),

$$n = n_i \exp\left(\frac{\frac{E_g}{2} - E_f}{KT}\right) \qquad (2.20a)$$

$$\sigma = Lq^2 N \frac{1}{(2\pi m^{*} KT)^{1/2}}\exp(-\frac{E_b}{KT}) \qquad (2.20b)$$

$$u = Lq \frac{1}{(2\pi m^{*} KT)^{1/2}}\exp(-\frac{E_b}{KT}) \qquad (2.21)$$

where n is the carrier concentration at the center of the grain, [22], n_i is the intrinsic carrier concentration, E_g is the band gap, σ is conductivity and u is mobility. Similarly the conductivity and mobility for the thermionic field emission can be written as,

$$\sigma = Lq^2 N \frac{1}{(2\pi m^* KT)^{1/2}} G \tag{2.22}$$

$$u = Lq\left(\frac{1}{2\pi m^* KT}\right)^{1/2} G \tag{2.23}$$

where G is defined as:

$$G = \int_E^{E_b} \exp\left(-\frac{E_b}{KT}\right) \tau(E) dE \tag{2.24}$$

The behavior of the barrier height and the mobility as a function of doping density are shown in Figures 2.3 and 2.4 for typical polysilicon with a grain size of 150Å and trap density of $5x10^{12}cm^{-2}$. These firgures are obtained by solving equations (2.3), (2.6), (2.21b) and (2.23).

It is important to know that equations (2.21) and (2.23) describe the ease of carrier motion from one grain to another in polycrystalline materials. This is referred to as effective mobility. It is not the familiar microscopic mobility related to the scattering in crystalline semiconductors. It only describes the restriction of the current flow by the grain boundary barrier. Although the effective mobility is frequently compared with measured Hall mobility, the theoretical relation between these two is not clear.

As noted earlier, an increase in the doping concentration results in an in

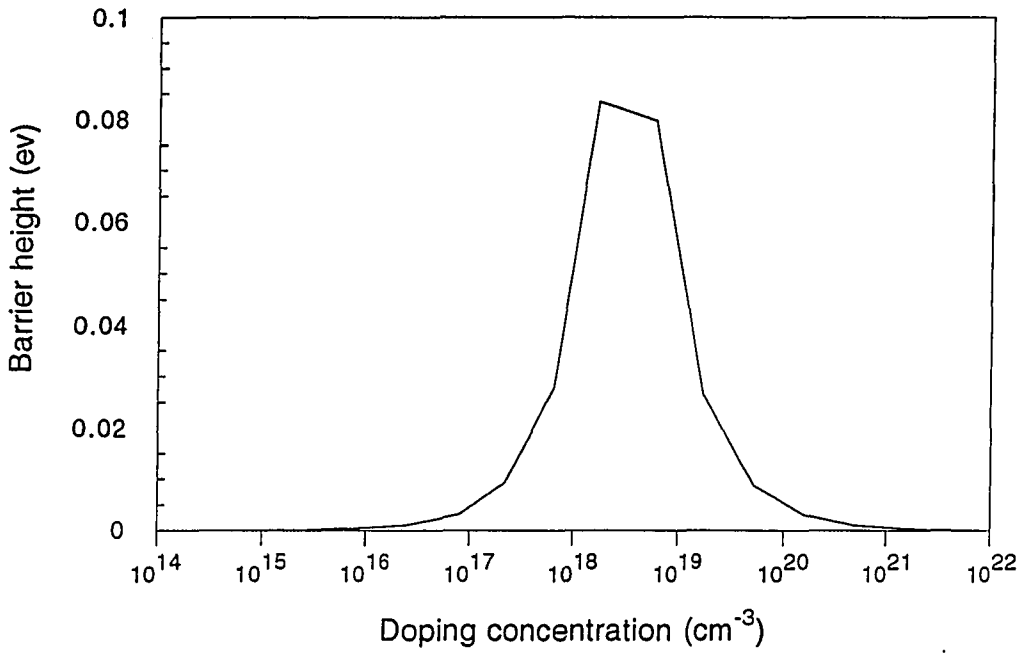

Figure 2.3 Barrier height vs. doping concentration

an increase in the barrier height at first, and then after reaching a maximum point at LN > N_T, the barrier height starts to decrease. Such a behavior results from the dipole layer created when impurity atoms are first introduced and the traps are being filled. The strength of the dipole atoms increases as the doping concentration increases and more traps are filled. However, after all traps are filled, the total charge in the dipole remains the same but the width of the dipole decreases which lowers the barrier height. The barrier height has a strong influence on the mobility in polysilicon, and consequently the mobility depends sensitively on the doping concentration as shown in Figure 2.4. The most dominant feature of the Figure (2.4) is the minimum mobility at about $10^{18}cm^{-3}$.

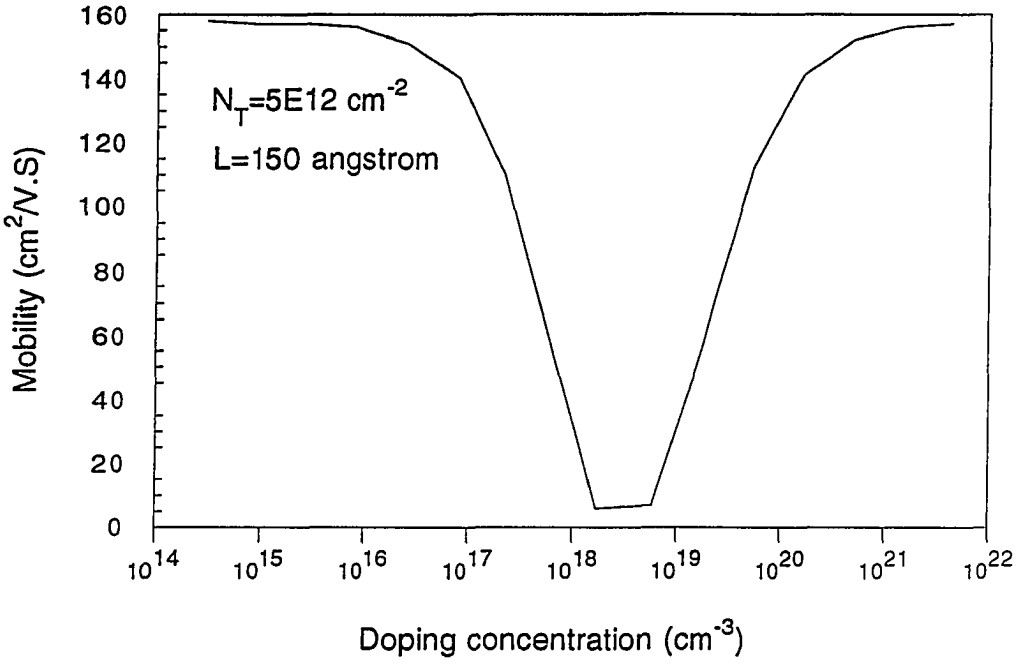

Figure (2.4) Electron mobility as a function of doping concentration

III. SAMPLE PREPARATION AND PLASMA CHARACTERIZATION

A. RPBE System

All samples reported in this study were deposited by using a reactive plasma beam epitaxy (RPBE) system. The operation of the RPBE system is based on creating an electron cyclotron resonance (ECR) condition. ECR is created when a moving particle in a magnetic field with a frequency of ω=qB/m is subjected to an electric field. The frequency of the electric field must be exactly equal to the frequency of the moving particle. Once the ECR condition is created the particles will be accelerated at each point of the orbit. Although the ECR condition can be generated at any frequency, such as the 13.5 MHz, used in a glow discharge, for most practical cases 2.45 GHz, is used. Lower frequencies result in very large orbits. This means more electrons can make the orbit without a gas phase collision, and hence the effect of resonance would be negligible [6]. Orbit radius and resonance frequency can be determined by applying Newton's second law and the Lorentz force shown below

$$F = qV \times B \tag{3.1}$$

$$F = mV^2/R \tag{3.2}$$

$$E = mV^2/2 \tag{3.3}$$

$$R = \sqrt{2mE} / qB \tag{3.4}$$

where q is electronic charge, V is the velocity, B is magnetic field intensity, R is the radius of the orbit, m is electron mass and E is the energy. Since the electrons are moving in a spiral path

$$V = 2\pi R / T \tag{3.5}$$

$$\omega_o = qB / m \tag{3.6}$$

where T is the period and ω_0 is the resonant frequency. From these relations, it is evident that particles with either larger mass or higher energy will have larger orbits. However, for the ions, the orbits are very large and they are usually ignored.

For a simple plasma, there exists a critical frequency. At or below that frequency, no wave can propagate in the medium. The relation between critical frequency, electron density and index of refraction can be derived by using Maxwell equations [23],

$$\omega = q\sqrt{N / \varepsilon m} \tag{3.7}$$

$$n = \sqrt{1 - \left(\frac{\omega_o}{\omega}\right)^2} \tag{3.8}$$

where ω_0 is the critical frequency, N is electron density, n is the refractive index, and ε is the permitivity of the free space. When $\omega > \omega_0$, the index of refraction is real and the wave is propagated. However, n is less than unity, so that refraction is opposite to that which occurs when the wave enters a denser

medium. When $\omega<\omega_0$ the index of refraction is imaginary and the wave can not propagate.

In a low pressure plasma, and in the absence of the magnetic field, a large fraction of energetic electrons travel through the plasma without making any ionizing collisions. Upon applying a magnetic field, it becomes possible for electrons to move in a spiral path, and hence increasing the path traveled many times. This results in more collisions with plasma species and consequently, a higher plasma density. In general an ECR plasma provides a denser plasma than magnetron and RF glow discharge. In addition, an ECR system is capable of operating at lower pressure (10^{-5} to 10^{-3} Torr). Higher pressure results in too many collisions for electrons to couple well with the microwaves. The collision frequency must be significantly lower than the driving frequency in order to have a good resonance.

Figure 3.1 shows the important components of the RPBE system. The 2.45 GHz microwave signal propagates from a microwave generator through a rectangular wave guide and a quartz window to an ECR source. The static magnetic field (875G) required for creating the ECR condition is provided by two DC powered electromagnets. The coil current is typically 190A for far chamber and 160A for the near chamber. Figure 3.2 shows the axial magnetic field magnitude as a function of distance.

Near the ECR source, a three stub tuner is located which can be used to optimize the reflected power. Hydrogen gas is introduced into the plasma source through a gas distribution ring near the quartz window. The process gasses are introduced through a three quarter inch opening near the substrate holder. A restricting orifice, with a 3 inch opening, defines the exit for the

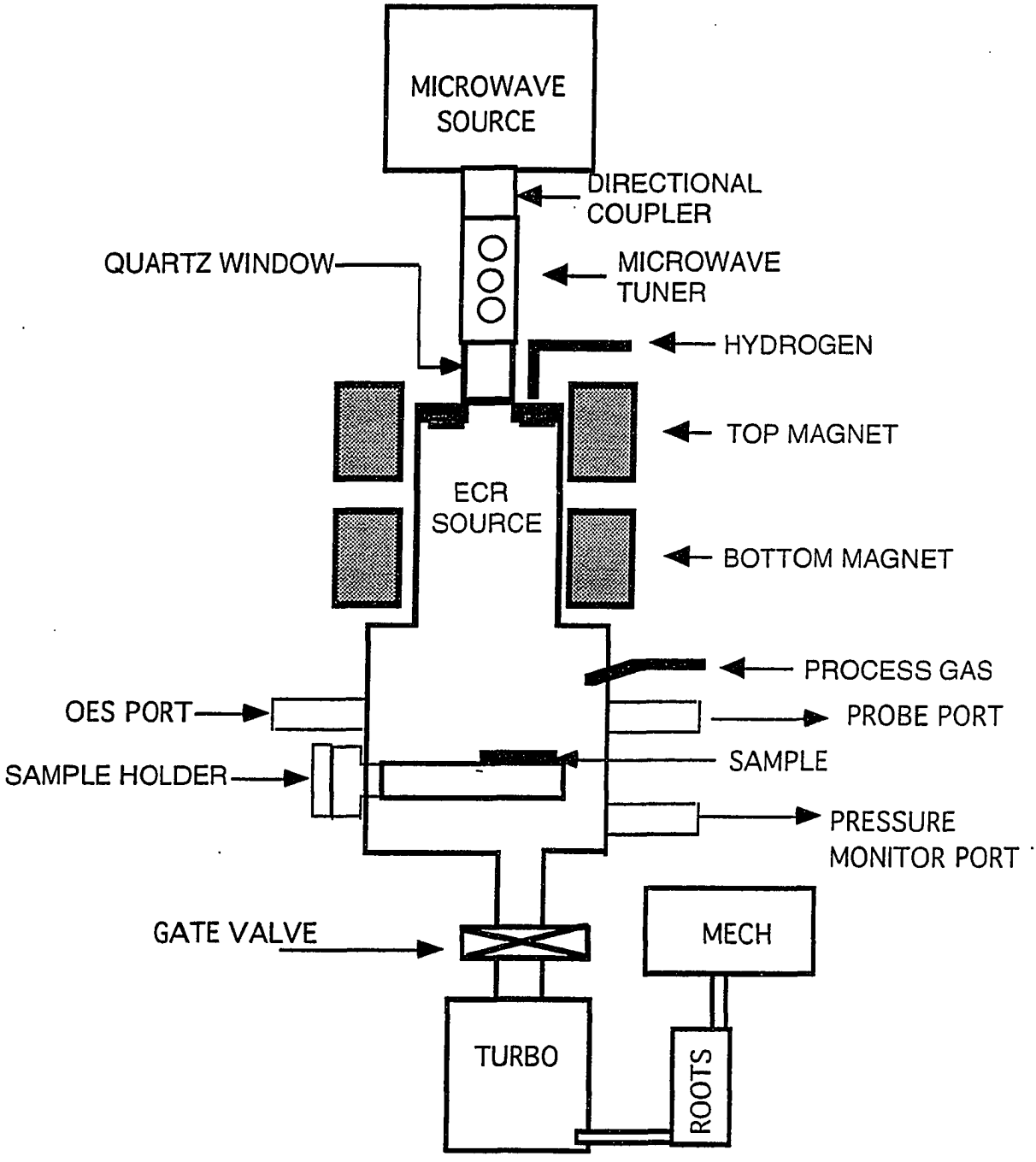

Figure 3.1 RPBE diagram

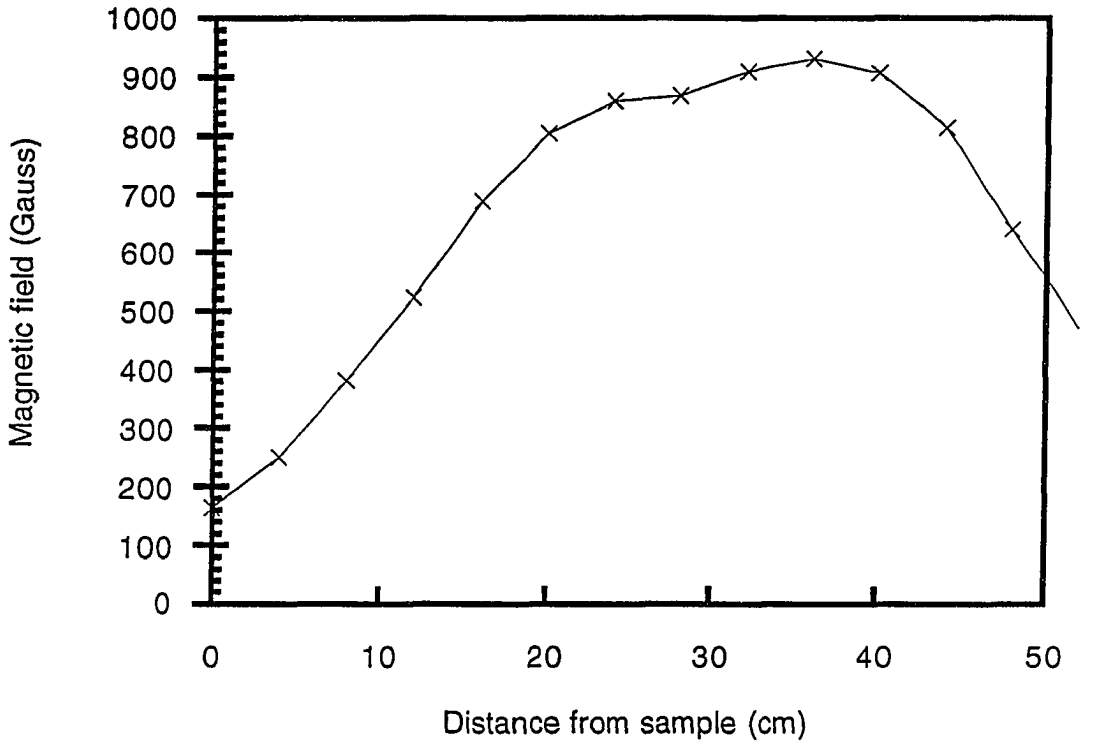

Figure 3.2 Magnetic field profile

plasma gas from the source and is located approximately four inch from the sample holder. To eliminate cross contamination during deposition, separate manifolds are used for the dopant and intrinsic gases. The substrate holder is made of stainless steel and is located some distance away from the plasma source. Substrates are clamped to the substrate holder and heated by cartridge heaters. The heaters are kept out of the vacuum chamber to reduce contamination. A shutter is placed in front of the substrate holder to cover the sample during the predeposition hydrogen etch. There are also several viewports on the deposition chamber. These ports are used for the plasma and

pressure monitoring.

Unlike conventional plasma enhanced chemical vapor deposition (PECVD), in an RPBE plasma, gas is excited some distance far from the deposition chamber. The process gases are injected down stream of the deposition chamber near the substrate holder, and therefore are not subject to direct plasma excitation. It has been shown that direct plasma excitation of silane leads to the formation of a number of potential gas phase depositions including SiH3, SiH, Si and H [13]. This means that some of the silane fragmentation products by themselves or in combination with other gasses generate unwanted bonding groups such as SiOH.

The vacuum necessary for the RPBE system is provided by two separate vacuum pumps. One consists of a turbomolecular-Roots combination and the other is a small mechanical pump which is in parallel with the first. If the main pump fails, the second pump will be able to pump the system safely. With this combination we have been able to obtain pressures below 10^{-7} Torr routinely. The loading and unloading of the samples is done by using a virtual load lock. In a virtual load lock, after the chamber is pressurized to atmospheric pressure the substrate holder is changed rapidly with a dummy cap, while maintaining argon or nitrogen with an appropriate flow rates through the chamber. A Virtual load lock is less troublesome than a real load lock.

Since the reactor uses toxic gasses a very careful safety system is implemented. The safety system of the RPBE reactor consists of:

1. A flow limit valve which is located on each cylinder right after the hand valve. This will shut off the cylinder in the case of a leak from a fitting.
2. A normally closed pneumatic valve which is placed after a flow limit valve.

This valve can be used to shut off the cylinder remotely.

3. Each cylinder is equipped with a regulator following a normally closed air actuated valve which can also be shut off remotely. In addition, each air actuated valve has a check valve after it so no gas can come back to the regulator.

4. After each mass flow controller, a normally closed valve is located. This will ensure that each gas line is off when it is required to be off.

In addition to these safety precautions there is also a main normally closed solenoid valve located on the gas manifold before the gasses enter the reactor. This valve is controlled by a solenoid which receives its electrical power from a Baratron pressure gauge. If the pressure of the reactor reaches 1T, the valve will not get its power from the gauge and consequently all lines will be shut off. This prevents the gas flow to the reactor when the vacuum system fails to operate properly.

B. Growth Chemistry

The growth chemistry of the polysilicon films is a fairly complicated process. In particular the role of the hydrogen and the dominant species responsible for film formation is still not clear. Three possible roles of hydrogen atom have been proposed to explain the growth of polysilicon films from the SiH_4/H_2 plasma:

1. Hydrogen atoms reaching the surface enhance the surface diffusion of radicals such as SiH_3 through a sufficient coverage of the film growing surface with hydrogen [24]. Based on this model, the amorphous structure of the films at lower temperatures is due to a decrease in the diffusion coefficient of SiH_x

radicals. This is because SiH_X radicals can not diffuse into stable sites for microcrystalline nuclei formation.

2. Hydrogen atoms act as an etchant to remove the weak bonds and provide a second chance for the Si atoms to be placed in the network [25].

3. Hydrogen atoms soak into several layers below the top growing surface which results in the promotion of network propagation (chemical annealing) [26].

The plasma induced silicon deposition follows a three step process which has been summarized by Dalal et. al [27] as:

1. Removal of surface H.

2. Insertion of SiH_3 molecules into the open bonds.

3. Removal of inter-atomic H and cross linking of Si atoms.

These steps are schematically shown in Fig. 3.3. In addition to these steps, statistical dynamics suggest that there will be extra atoms (hills) and voids (valleys) in the grown films. Therefore, they concluded that to smooth out the hills and the valleys, surface mobility of Si atoms and SiH_3 molecules must be enhanced. This can be done by three different methods:

1. Increasing substrate temperature.

2. Providing extra energy to the growing surface.

3. Etching during the growth and in-situ annealing.

The first technique is not suitable for the VLSI and ULSI circuits. This is because it can cause auto diffusion. However, by combining the second and the third method, the quality of the polysilicon films can be significantly improved without any side effects. This can be done by subjecting the growing surface to the hydrogen flux with a uniform and moderate energy, in the range

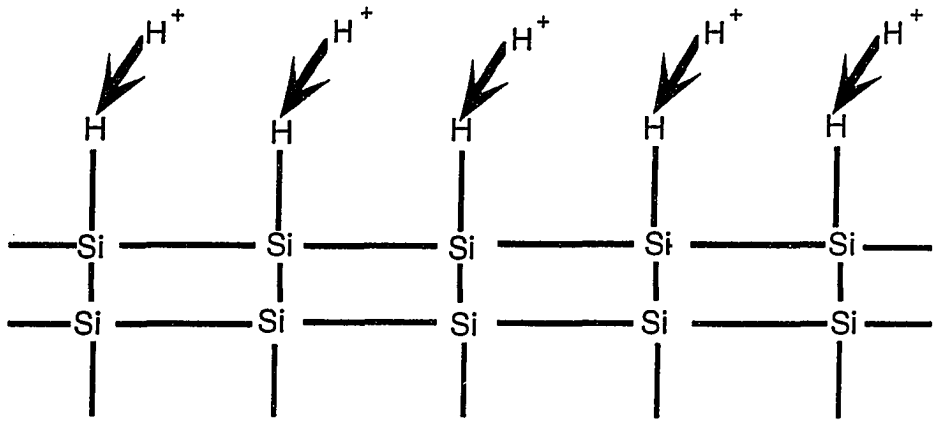

H elimination

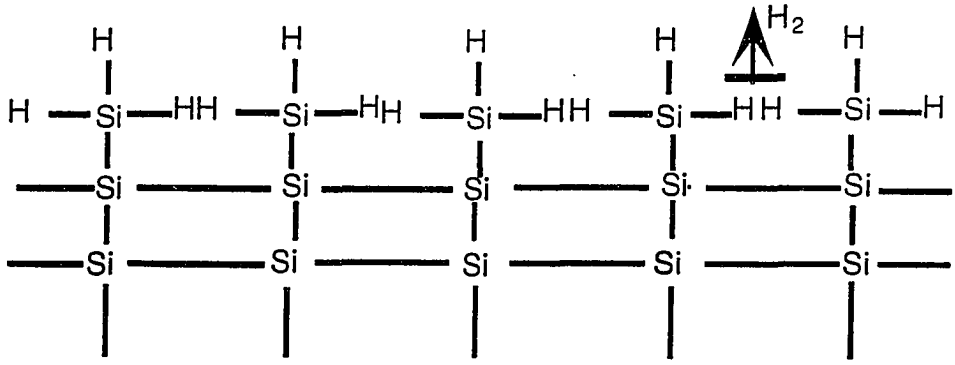

SiH_3 Insertion

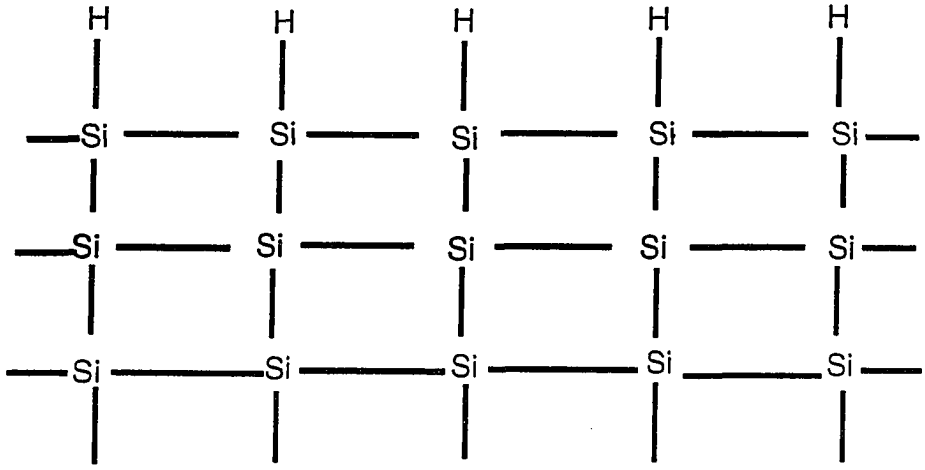

Figure 3.3. Chemical steps in formation of Si

of a few eV. This technique not only etches the weak bonds, but also allows more silicon atoms to cross link, because silane radical species can diffuse further due to higher surface temperature. The idea of increasing the surface mobility and in-situ chemical etching is the basis for the development of an RPBE system.

C. Film Structure

Once silane radicals reach the substrate, the absorbed atoms on the surface will migrate further and produce nucleation. An adsorbed silicon atom which has been diffused randomly can also be desorbed or evaporated. Since these atoms are weakly bonded to the surface, they can also encounter the other silicon atoms and form an atomic pair. Because of the large atomic mass, it is less likely that this pair desorbs. Additional diffused silicon can join this pair and form a cluster.

The cluster finally reaches a size which beyond that it is unlikely to desorb and become a stable nucleus on which the deposition continues. The size of the cluster is determined by pressure, temperature and the binding energy between the atoms in the cluster [1]. As the number of the nuclei increase, it is more likely that the incoming atoms will be adsorbed by the existing nuclei rather than the forming a new one. This process continues until nuclei reach the saturation value after which they remain relatively constant. In an RPBE system we believe that the critical size of the cluster is determined mainly by pressure. The ability to grow amorphous, microcrystalline and polysilicon films at the same temperature and power supports this idea.

D. Sample Preparation

In this research project, we have deposited polysilicon films on 7059 Corning glass substrates and silicon dioxide (SiO_2). Glass substrates were first cleaned before loading to the system. The cleaning process consists of a 20 minute acetone cleaning followed by 20 minutes of methanol and 20 minutes of alcohol cleaning. Glass substrates were then dried by N_2 and kept in a storage box. The SiO_2 substrates were prepared by using p-type silicon wafers with a resistivity of 1-10 ohm-cm and (100) orientation. An oxide thickness of 0.4 micron was obtained after 40 minutes of wet oxidation at 1100 ^oC. Prior to oxidiation silicon wafers were RCA cleaned. Following is a procedure that we used for the cleaning:

1. Removing residual organic contamination and certain metals in H_2O-NH_4OH-H_2O_2 (5:1:1) at 75-80 ^oC.
2. Over quenching of the solution by placing the wafers in running DI water for 5 minutes.
3. Stripping off the hydrous oxide by (50:1) H_2O-HF for 15 seconds.
4. Removing the HF solution by inserting the wafers in running DI water for one minute.
5. Desorption of the remaining atomic and ionic contaminants by preparing H_2O-HCl-H_2O_2 (6:1:1) for 15 minutes at 75-80 ^oC.
6. Over flow quenching of solution in DI water for 5 minutes.
7. Drying the wafers by N_2 using plastic tweezers.

E. Deposition Parameters

All samples in this investigation were grown using a hydrogen plasma. The substrate size was 1.2 by 1.2 inch and the deposition temperature varied from 400 to 550 ^{o}C. To assure that the temperature on the surface of the samples has indeed reached the predetermined value, the deposition was always started at least one hour after the samples were loaded. The sample holder was always grounded during the deposition period. Two methods were used to optimize the plasma before deposition. The first method involves adjusting the three stub tuner for obtaining the minimum reflected power while the current of the top and the bottom magnets was kept at 190A and 160A respectively. The reflected power for this method was as low as a few watts. In the second method, stub tuners were kept unchanged while the magnet currents were varied for maximum plasma intensity. For this method the reflected power was ranging from 20 to 50% of the incident power. Better reproducibility was obtained using the second method.

Typical flow rate for H_2 was 36 standard cubic centimeters per minute (sccm) and for SiH_4 in the range of one sccm. The deposition rate for intrinsic films was 1.4 Å/min and the thickness of all intrinsic films were in the range of 1 micron. 1% B_2H_6 in H_2 was introduced to the chamber for growing p type films. Silane, hydrogen, and B_2H_6 flow rates were 1,36 and 6 sccm respectively. Two types of diluted PH_3 gas was used for n type samples. 10 ppm PH_3 diluted in argon and 100 ppm PH_3 diluted in H_2. Flow rates for PH_3 diluted in H_2 were 0.6 to 3 sccm and for argon diluted was 2-5 sccm. Table 3.1. is a summary of all parameters used for polysilicon growth. The incident power was 100-200W and the pressure was 6-7mT.

Table 3.1. Typical deposition parameters

Parameter	Range
SiH_4	1sccm
PH_3 in H_2	0.6-3 sccm
PH_3 in Ar	2-5 sccm
B_2H_6 in H_2	6 sccm
Temp.	400-550
Pressure	6-7mT
Incident power	100-200W

F· Plasma Characterization

Langmuir probe and optical emission spectroscopy (OES) were used to study the influence of power, pressure and flow rates on the plasma properties.

1. Langmuir Probe

The Langmuir probe is the most common plasma diagnostic technique. In this method, a metal wire is inserted in the plasma and the current in the wire is monitored as a function of an applied voltage. In our system the probe is placed in parallel and with a distance of one inch from the substrate. The probe that we used is an 8mm diameter disk shape. The back side of the probe was coated with boron nitride which is an insulating material. In order to eliminate

the possibility of the effect of silane deposition on the probe, it was cleaned by potassium hydroxide after each measurement.

Figure 3.4 shows the variation of current versus the probe potential. At $V=V_S$ the probe is at the same voltage as the plasma. Therefore, the net electric field on the surface of the probe is negligible and the particles migrate to the probe because of their thermal velocities. Since the mass of an electron is much smaller than an ion, the collected particles are predominantly electrons. Now if the probe is made positive with respect to the plasma potential, electrons will be accelerated toward the probe and ions will be repelled. This eliminates the little ion current that was present at $V= V_S$. In this situation there exists an excess number of negative charges on the surface of the probe. This layer of the charge, which is referred to as sheath, is very thin with little electric field. This means that the plasma is not disturbed. As the probe voltage increases there is little increase in the electron current. This is because the thickness of the sheath is relatively constant and only electrons with enough thermal energy can reach the probe. This portion of the curve (part A on Figure 3.4), known as the saturation region, is fairly constant.

If the probe potential is made negative (with respect to the plasma potential) electrons begin to repel and ions will accelerate towards the probe. The electron current falls as the curve reaches part B. At $V=V_f$ (floating potential) the probe is sufficiently negative and repels all electrons except a flux equal to the flux of ion and, therefore, draws no current. As the negative voltage is further increased, all electrons will be repelled and the result would be an ion current, designated as Part C on Figure 3.4. Once the I-V curve is measured, we can calculate local plasma density, electron density, electron temperature,

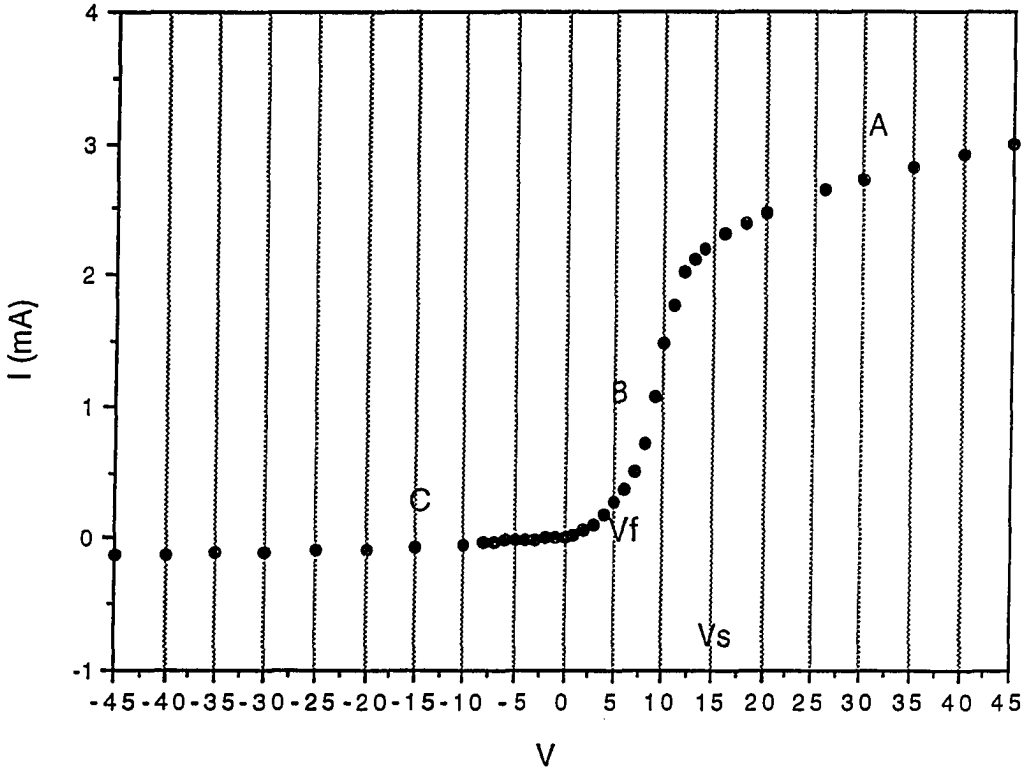

Figure 3.4 I-V curve

space potential and ion density. In general, the current collected by the probe is

$$I = qNAV / 4 \tag{3.8}$$

where q is electronic charge, A is the area of the probe, N is electron density and V is the velocity. If we assume that the electron distribution is Maxwellian [28] then we can write the velocity as

$$v = \sqrt{\frac{8K_B Te}{\pi m}} \tag{3.9a}$$

For thermal equilibrium distribution the electron density is determined by the Boltzmann factor

$$N = N_{\infty} \exp\left(\frac{qV}{KT}\right) \tag{3.9b}$$

where N_{∞} is the electron destiny far from the perturbing charge where V is zero Substituting equation (3.9b) in (3.8) results in

$$I = ANqV_e \exp(qV / K_B T_e)$$
$$\ln I = C + qV / K_B T_e \tag{3.10}$$

where C is the pre exponential constant, V is the voltage, V_e is the electron velocity, k is the Boltzman constant and T is electron temperature in Kelvin. If we plot ln(I) vs. voltage the inverse of the slope is the electron temperature. Figure 3.5 is a plot of ln(I) vs. applied voltage. Once the electron temperature is calculated it is a simple task to determine the electron density by using

$$N = \frac{I_{eo}}{Aq}\sqrt{\frac{2\pi m}{K_B T_e}} \tag{3.11}$$

where I_{eo} is the electron current at the knee of the curve in Figure 3.5. Ion current can be extrapolated from a line which is fitted to the ion current in part C of the Figure 3.4. If we assume that $T_i << T_e$ then the ion acoustic velocity Vi can be written as [28]

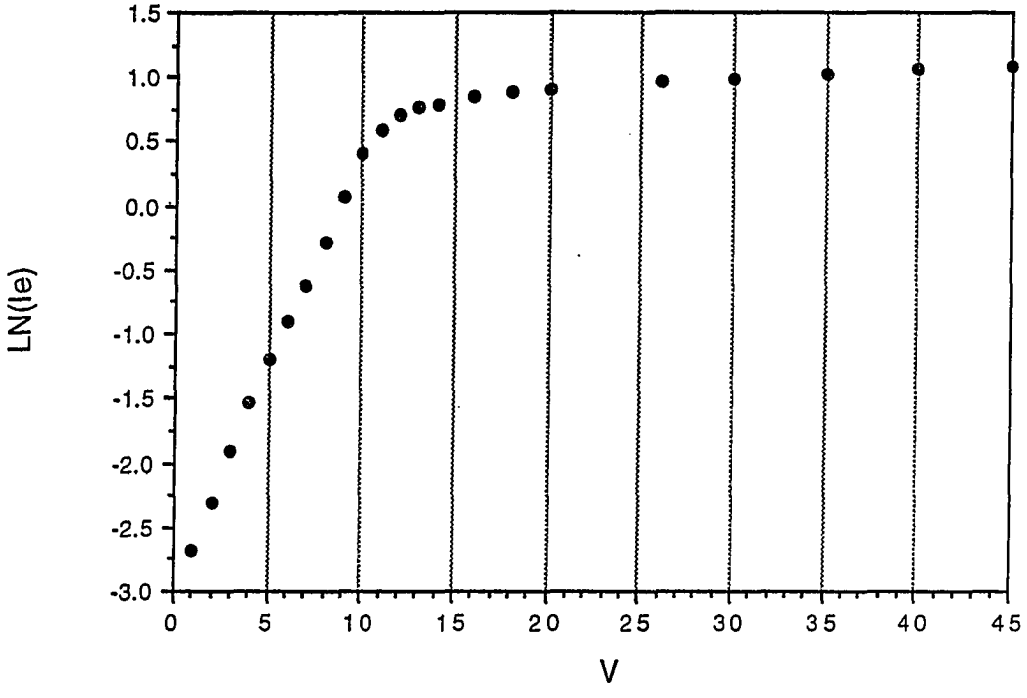

Figure 3.5 LnI vs. Voltage

$$Vi = \sqrt{\frac{K_B T_e}{m_i}} \tag{3.12}$$

Ion density can be calculated from the relation

$$N_i = \frac{I_i}{qAV_i} = \sqrt{\frac{m_i}{K_B T_e}} \tag{3.13}$$

where Ni is ion density I_i is ion current and m_i is the ion mass. Equation (3.13) is independent of the ion temperature.

The following conditions must be satisfied in order to be able to extract electron density, electron temperature, and other plasma parameters from I-V measurements:

1. The Electron distribution must be Maxwellian .
2. The effect of magnetic field and secondary electrons must be negligible.
3. The plasma density has to be high enough so that the size of the sheath is small compared to the probe dimensions.
4. Surface must be clean.
5. Electron neutral collision length has to be large compared to the probe dimensions.

2. Optical Emission Spectroscopy

Optical emission spectroscopy (OES) is a technique which analyzes the light emitted from plasma. When excited atoms and molecules in a plasma relax from one energy level to another, they emit a series of spectral lines that are unique for each species. By using OES technique the effect of the plasma parameters on the film deposition can be qualitatively studied.

Our OES set up is mounted on one of the view ports on the deposition chamber. It consists of a monochromator, a chopper, a lens, a photo diode, a lock in amplifier and an active filter. Figure 3.6 shows the block diagram of the OES system. Light from the plasma goes through a monochromator. A monochromator is very similar to an optical filter which can transmit a fixed band of wavelengths. The function of the chopper is to eliminate any ambient or other radiation that might interfere with the incoming light from the plasma source. The collimated lens, which is located after the chopper will focus the light to the photodiode. The photo diode used in this set up is a silicon

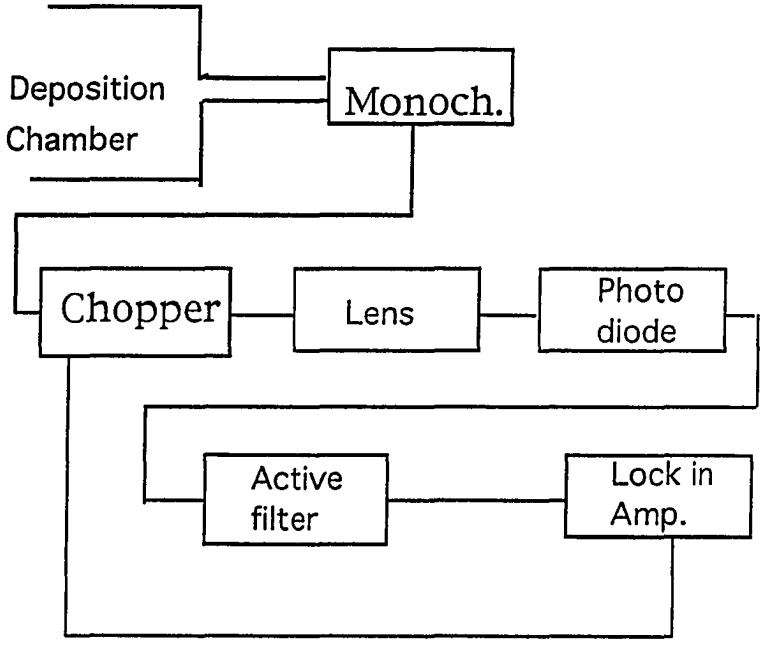

Figure 3.6 OES Set up

photodiode. The spectral response of a silicon diode covers the visible and the near infrared region. The lockin amplifier serves as both a narrow band amplifier and a phase sensitive detector. If the bandwidth of the noise is larger than the original signal then the noise will be eliminated resulting in better signal to noise ratio. For a lock in amplifier to be really useful, the signal must be modulated at some frequency within the range of the lock in amplifier while the noise must be kept unmodulated. A chopper can be used as a simple modulation device. For further improvements in the quality of the signal and reducing the noise associated with the microwave, we have also used an active filter.

IV. CHARACTERIZATION TECHNIQUES

The deposited samples were analyzed by a variety of characterization techniques. These include optical, structural, compositional and electrical characterizations.

A. Optical Characterization

Optical characterization is important in a number of polysilicon applications. For example, in charge coupled device (CCD) image sensors, light must often pass through a polysilicon electrode gate into an underlaying sensing region [1]. In polysilicon solar cells, light must be properly absorbed for efficient photovoltaic conversion.

The optical properties of polysilicon, to some extent, are different than crystalline silicon because of the defects in the grain boundary region. The defects are active recombination centers, and hence, they can absorb light with an energy less than the band gap energy. Moreover, scattering due to the existence of grain boundaries can cause significant changes in the optical properties.

The basis for most of the optical measurements is the response of the medium to an electromagnetic wave, which is described by the complex dielectric constant [29]

$$\tilde{\varepsilon} = \varepsilon_R + i\varepsilon_I \tag{4.1}$$

The index of refraction and absorption coefficient are related to the dielectric

constant by:

$$\sqrt{\varepsilon} = n + ik \tag{4.2}$$

where n is the index of refraction and k is the extinction coefficient. This is defined as

$$k = \lambda\alpha / 4\pi \tag{4.3}$$

Therefore, knowledge of the index of refraction and absorption coefficient is essential in order to determine the optical properties of the deposited films. All optical calculations reported in this study are based on the transmission, absorption and reflection spectra obtained from a Perkin Elmer visible/uvIR Spectrophotometer. The spectrophotometer is controlled by an IBM micro-computer and utilizes a software referred to as λ-9.

1. Film Thickness and Index of Refraction

The thickness of a thin film semiconductor can be determined by maxima and minma resulting from the constructive and destructive interference. It is well known that the phase of a propagating electromagnetic wave varies with position according to:

$$E = E_0 \exp[i2\pi f(t - (x / V)] \tag{4.4}$$

Here f is frequency of the propagation, V is velocity, and t is time. If the sample has a thickness of x, the phase of the propagating wave changes by [30].

$$\theta = 2\pi f \frac{x}{v} \tag{4.5}$$

Where:

$$v = \frac{n}{c}$$
$$f = \frac{c}{\lambda} \tag{4.6}$$

Substituting (4.6) into (4.5) results in

$$\theta = 2\pi \frac{n}{\lambda} x \tag{4.7}$$

For constructive interference the phase change of the reflected wave will be 3θ, 5θ etc., therefore the thickness can be determined by

$$x = \frac{(2m+1)\lambda}{2n} \tag{4.8}$$

In the case of destructive interference, the phase change will be 2θ, 3θ, etc., and the thickness will be:

$$x = \frac{(2m+1)\lambda}{4n} \tag{4.9}$$

Using these relations, film thickness at two adjacent extrema can be determined by:

$$x = \frac{1}{2n(1/\lambda_2 - 1/\lambda_1)} \tag{4.10}$$

This method is applicable when the index of refraction is known and it is constant in the range of interest. For single crystalline silicon, the index of refraction is constant in visible region (400-800nm). Kuhl et. al [31] have shown that the extinction coefficient of crystalline silicon is significantly different from polysilicon, particularly for highly doped films. Therefore, knowledge of the refractive index is essential for calculation of the thickness for both doped and undoped polysilicon films. A number of papers have dealt with modeling and calculating the index of refraction for amorphous and polysilicon films [32, 33,34,35]. In this study we have used the model suggested by R. Swanepoel [33]. In his method, the transmission spectrum of the film, obtained from a spectrophotometer, is assumed to be a continuos function of wavelength. Once the minimum and maximum points are determined from this function, which is the envelope of the transmission spectrum, the index of refraction and the thickness can be calculated by using the following equations:

$$n = \left[N + \left(N^2 - S^2\right)^{1/2}\right]^{1/2} \tag{4.11}$$

where N is defined by:

$$N = 2S\frac{T_M - T_m}{T_M T_m} + \frac{S^2 + 1}{2} \tag{4.12}$$

$$X = \frac{\lambda_1 \lambda_2}{2(\lambda_1 n_2 - \lambda_2 n_1)} \qquad (4.13)$$

T_m and T_M are the maximum and minimum points on the envelope of the transmission spectrum and s is the index of refraction of the substrate. Equation (4.13) is sensitive to errors and gives only an estimate of the thickness. Knowledge of the approximate layer thickness establishes the exact value of m, and thus an accurate thickness can be obtained by equation (4.14).

$$2nX = m\lambda \qquad (4.14)$$

We have also used a profilometer to cross check the accuracy of the thickness obtained from equation (4.14). The thickness measured by using the profilometer was always about ten percent lower.

2. Absorption Coefficient

The absorption coefficient is another optical parameter that provides valuable information about the structure and the band gap of semiconductor materials. Absorbance of the transparent samples is measured by a Perkin Elmer Spectrophotometer and then by using the equations (4.15) and (4.16). The absorption coefficient was calculated using

$$\Gamma = \frac{1 - 2n + n^2 + K^2}{1 + 2n + n^2 + K^2} \qquad (4.15)$$

where Γ is the reflection coefficient, n is the index of refraction and K is extinction coefficient. Once the values of absorbance and reflection coefficient are known, the absorption coefficient can be determined by equation (4.16).

$$\alpha = \frac{2.306[A + LOG(1-\Gamma)]}{X} \qquad (4.16)$$

Here α is absorption coefficient, X is the thickness of the film, A is absorbance obtained from the spectrophotometer, and Γ is the reflection coefficient.

The band gap of the deposited films is deduced from the data of the absorption coefficient. Considering polysilicon as an indirect band, where quantum selection rule forbids the direct transition at K=0, then the absorption coefficient is proportional to $(E_g\text{-}h\upsilon)^{1/2}$ [29]. Since the value of the absorption coefficient is already determined from the measured absorbance spectrum, energy gap can be obtained from a plot of $\sqrt{\alpha}$ vs. hυ.

B. Structural Evaluations

To assure that the deposited films are indeed polycrystalline, structural properties of the samples are studied by several different analysis techniques. These include Raman spectroscopy, x-ray diffraction and UV reflectance measurements.

1. Raman Spectroscopy

Raman spectroscopy is a powerful technique which has been widely applied to the characterization of semiconductor materials. This is because it offers a nondestructive and quantitative microanalysis of the structure of the

semiconductor materials. The basis for the Raman scattering is the interaction of incident light with optical phonons. When the incident photon gives its energy to the lattice in the form of an optical phonon, the frequency of the incident beam will be changed to account for the lost energy. This process is known as Stokes scattering. If the scattered light frequency is larger than the frequency of the incident laser beam then the result is anti Stokes shifting. Stokes shifting occurs when the scattered light frequency is lower than the frequency of the laser beam. Principles of Raman scattering as well as its applications in the field of the semiconductor are thoroughly reviewed in references [36, 37,38].

The Raman spectroscopy measurement was performed in the Chemistry Department at Iowa State University. The scattering system used in this project consists of a triple spectrometer 1877 Spex equipped with an intensified 1463 PAR diode array. An Innova 100 (coherent) Ar^+ ion laser was applied for excitation of Raman spectra. The laser wavelength was 514.5nm at a power of 30 mW. A backscattering geometry was used and the scattered light was collected by an F/1.2 camera lens.

2. X-ray Diffraction

A Read camera and x-ray diffractometer were used to measure the crystallinity, grain size, and orientation of the deposited films. The basis for x-ray diffraction is Bragg's law

$$n\lambda = 2d\sin\theta \qquad (4.17)$$

where λ is the wave length, d is interplane distance, θ is the diffracted angle

and n is the diffraction order. When x-rays encounter a crystalline structure, they are diffracted by the planes of the atoms within the crystal. The diffracted angle, θ, depends upon the wave length and the distance between planes.

In the case of the Read camera, the x-ray pattern is obtained by impinging the sample with a beam of light coming from an x-ray monochromator. The collimated beam is directed at the sample through two pinholes; patterns of all angles are then recorded on a film placed some distance from the center.

The grain size and the texture of the polysilicon samples were determined by a Siemens D500 diffractometer at the Material Analysis and Research Laboratory in the Department of Civil and Construction Engineering at Iowa State University. The overall configuration of the diffraction system is shown in Figure 4.1. The diffractometer is normally controlled via a LC500 interface by using a PDP 11/23 microcomputer.The computer offers bulk storage of raw data on 8 inch floppy disks. The PDP 11/23 computer can be connected to an AT Clone computer that can access the JCPDS search-match This allows a quick identification of unknown powder diffraction patterns.

The orientation of the polysilicon films was determined by matching the 2-theta angle obtained from the diffractometer with the standard value for crystalline silicon. The raw data was corrected for the thickness of a sample by dividing the intensity with the correction factor obtained from equation (4.18) [39]

$$G = 1 - \exp\left(\frac{-2ut}{\sin\theta}\right) \qquad (4.18)$$

where G is the correction factor, u is the absorption coefficient (reciprocal of

absorption length), t is the thickness of the sample and θ is the Bragg angle. The absorption lengths of the common Fe K_α and Cu K_α x-rays in silicon are 38 and 71 um respectively. The correction factor should be used when the thickness of the film is several times smaller than the absorption length.due to the fact that not all the x-rays are absorbed and diffracted within the sample. The grain size was calculated from the line width (full width half maximum of the x-ray spectra) by applying equation (4.19), known as the Scherrer formula

$$L = \frac{k\lambda}{B_{1/2}\cos\theta} \tag{4.19}$$

where k is a constant in the range of 0.8 to 1.3 and in most cases 0.9, λ is the x-ray wavelength (1.541838Å) for Cu K_α radiation, θ is the Bragg angle and B is

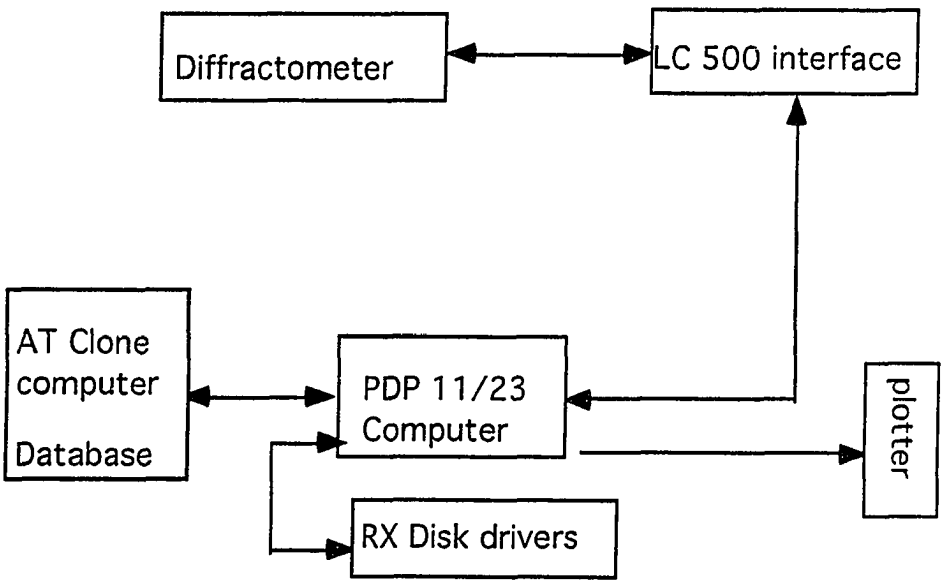

Figure 4.1 Configuration of Siemens D500 diffractometer data base

the line width. The derivation of the Scherrer's equation as well as its range of validity and practical consideration in applying this equation can be found in references [40,41]. The measured linewidths were corrected for instrumental broadening by measuring a standard silicon powder and applying the Warren method [40].

3. UV Reflectance

The UV reflectance measurement is a quick, qualitative, and nondestructive technique that can be used to confirm the crystallinity of the deposited samples. The basis for the UV reflectance analysis is the interband transition. It is well known that for crystalline silicon there are two peaks at 280nm (4.4eV) and 365nm (3.4eV). They are caused by optical transitions at X point and along the Γ-L axis of Brillouin zone respectively [42]. These maxima can still be seen in the curve taken for polysilicon, while they are missing in the amorphous materials.

C. Surface Morphology

Surface roughness is an important factor in integrated circuit technology. In particular, for sub-micron processes the surface of polysilicon films must be smooth enough to define patterns by standard photolithography method. Optical techniques are the most common methods used for the surface analysis of semiconductors because of their high sensitivity, accuracy and contactless nature. Surface morphology of the samples was analyzed by two different methods, scanning electron microscope (SEM) and UV reflectance method. A Cambridge steroscan 200 SEM was used to study the effect of the dopants and deposition temperature on the surface morphology of the grown films. UV

reflectance spectrums obtained from the spectrophotometer were used to determine the surface roughness of the deposited samples.

Since short wavelength < 400nm can not penetrate silicon films (because of high absorption), the reflectance spectrum can be a good signature of the surface properties of the silicon films. This concept can be used to develop an analytical relation from which the root mean square (RMS) of surface value can be calculated. [43]

$$\frac{R_{poly}}{R_{Si}} = \exp -\left(4\pi\cos\theta\,{}^{\sigma_0}/_{\lambda}\right)^2 + \frac{32\pi^3\cos^3\theta\Delta\omega\left({}^{\sigma_0}/_{\lambda}\right)^4}{m^2} \qquad (4.20a)$$

For $\sigma/\lambda << 1$

$$\frac{R_{poly}}{R_{Si}} = \exp -\left(\frac{4\pi\cos\theta\sigma_0}{\lambda}\right)^2 \qquad (4.20b)$$

$$\sigma_0 = \frac{0.12\lambda}{\cos\theta}\sqrt{\log(R_{Si}/R_{poly})} \qquad (4.20C)$$

Where σ_0 is RMS value of surface roughness, λ is the wave length, θ is the angle of incident beam, $\Delta\omega$ is the solid angle of observation, R_{Si} is reflectance of an ideally smooth surface of the same material (in this case silicon) and R_{poly} is the reflectance of the sample. If we plot $\log(R_{Si}/R_{poly})$ versus $1/\lambda^2$, the RMS value of the surface roughness can be computed from the slope of such a plot.

D. Compositional Analysis

Depth profiles of phosphorus, hydrogen and oxygen were measured by secondary ion mass spectroscopy (SIMS). The SIMS technique is based on the removal of materials from the sample by sputtering and analysis of the sputtered materials by a mass spectrometer. More detailed discussion on the theory, application, and the instrumentation of the SIMS can be found in the reference [45].

E. Electrical Characterization

Electronic properties of the deposited films were characterized by the means of resistivity measurement, Hall mobility and activation energy. To examine the dominant carrier transport and the intergrain tunneling, conductivity and Hall mobility as a function of temperature was also measured.

Resistivity and Hall mobility of all films were measured by the Van der Pauw technique. A single measurement of this type provides information about resistivity, carrier concentration and mobility. In the case of resistivity measurement, the principal advantage of this method over two point probe is that the current and the voltage measurements are decoupled, which minimizes the effect of the contact resistance. The theoretical foundation of the Van der Pauw method is based on the conformal mapping developed by Van der Pauw [44]. This method requires a singly connected specimen (without any pinholes), and homogenous in thickness. The contacts must be ohmic and placed at the periphery of the sample. To minimize the effect of interferences on the measurements the following precautions were made:

1. All measurements were performed in the dark to eliminate the possibility of

the photovoltaic effect.

2. The linear current voltage relation of all contacts was examined in the range of interest prior to the measurement. This would alleviate the effect of minority current injection during the measurement.

A complete list of all necessary precautions can be found in standard test methods for measuring resistivity and Hall coefficient in single crystalline semiconductors printed by American Society for Testing and Materials documented under F 76-86.

Aluminum dots were thermally deposited on the four corners of the intrinsic and phosphorus doped films by using a shadow mask. For boron doped samples, nickel was used as the contacts. The selection of the metals for contacts is based on the matching of the work function of the metal and the semiconductor. Proper material selection is critical for providing good ohmic contacts. All samples were prepared in a of 1x1 cm^2 square. The diameter of the metal contacts was always less than 5% of the sample dimensions. For resistivity and mobility measurements, current was passed through two contacts and voltage was measured across the other two contacts. For each measurement the current polarity was reversed and the voltages in both directions were averaged for calculating the conductivity, mobility and carrier concentration.

1. Resistivity Measurement

Resistivity of all samples was calculated by the following relations, [44]

$$\rho_A = \frac{\pi t f_A}{4 \ln(2) I} \qquad (4.20)$$

$$\rho_B = \frac{\pi t f_B}{4\ln(2) I} \tag{4.21}$$

$$\rho_{ave} = \frac{\rho_A + \rho_B}{2} \tag{4.22}$$

where ρ_A, ρ_B, are the resistivities for the positive and negative currents respectively, ρ_{ave} is the average resistivity, f is the correction factor calculated by using equation (5.21) suggested in Ref [45] and t is the specimen thickness.

2. Hall Mobility

Hall effect measurements were carried out to determine the mobility as well as the average carrier concentration. The measurement was performed by using a conventional Van der Pauw set up. The basis for Hall effect is the experiment devised by E. H. Hall, in which a strip of material to be studied is placed in a magnetic field. By measuring the electric field resulting from the current passing through the strip, the mobility as well as the carrier type in the material can be determined. More detailed discussion of the Hall effect can be found in reference [46].

The polysilicon samples, which were prepared in $1cm^2$ square shapes, were mounted on a printed circuit board and then clamped to an aluminum block. The aluminum block was used to heat up the films when necessary. The temperature was monitored by a surface mount thermocouple under the sample. The Hall coefficient was found by using eq. (4.23), and the Hall mobility was calculated by using eq. (4.24).

$$R = \frac{tdV}{dBI} \tag{4.23}$$

$$u = \frac{|R|}{\rho_{ave}} \tag{4.24}$$

Where t is the thickness, V is Hall voltage, B is magnetic field, R is the Hall coefficient and u is mobility

3. Activation Energy

To examine the effect of the deposition parameters on the position of Fermi level, an Arrhenius plot was drawn and the slope of the plot was used to estimate the position of the Fermi level. For activation energy measurements, coplanar aluminum or nickel contacts were thermally evaporated on the samples. Then the current of the sample was monitored while it was heated up to 200 ^{o}C. Equations (4.25) and (4.26) were used to determine the behavior of the conductivity as a function of temperature.

$$\sigma_1 = \sigma_0 \exp(-q\Delta E / kT_1) \tag{4.25a}$$

$$\sigma_2 = \sigma_0 \exp(-q\Delta E / kT_2) \tag{4.25b}$$

$$\Delta E = \frac{10^3 k \ln\left(\frac{\sigma_2}{\sigma_1}\right)}{q\left(\frac{10^3}{T_1} - \frac{10^3}{T_2}\right)} \tag{4.26}$$

Where σ is the conductivity, E is the energy, k is Boltzman constant, T temperature in Kelvin and, ΔE is the activation energy.

V. RESULTS AND DISCUSSION

The optical and electrical properties of polysilicon films depend highly on the plasma parameters. The deposition system for producing polysilicon films suitable for integrated circuits must fulfill certain conditions such as high deposition rate, large grain size, high conductivity, high mobility, reasonable film uniformity and surface roughness. To obtain uniform films at high deposition rates, the plasma stream must have a large ion density and a high electron temperature. The latter is important because a high degree of decomposition of silane near the substrate is required for a high deposition rate. Moreover, enough energy must be provided to the surface of the growing film so that the weak bonds are removed from the surface allowing the nucleation sites to expand. Based on these considerations and the results that we obtained from the Lagmuir probe and optical emission spectroscopy, polysilicon films in this study were prepared at an incident power of 200W and pressures between 6-7mT.

At such a low pressure, the hydrogen radicals have a long mean free path and can travel to the substrate with little recombination. At the substrate, these hydrogen radicals combine with silane and produce silyl (SiH_3) radicals which then lead to film growth. In addition, since the H-Si bond is stronger than the weak Si-Si (e.g. amorphous Si) bonds, hydrogen radicals can be used to preferentially etch away amorphous Si during growth, leaving behind primarily crystalline Si bonds. Thus, we can promote crystallinity even at low temperatures by controlling the flux of H radicals.

A. Plasma Characterization

1. Langmuir Probe

A series of Langmuir probe measurements were carried out to examine the plasma properties. Typical Langmuir probe data is shown in Table 5.1. Data was collected at pressures ranging from 7 to 20 mT, and incident powers from 100 to 200 W. For all cases, the electron density was found to be larger for the magnet optimized plasma compared to tuner optimized plasma. Figure 5.1 illustrates the effects of pressure and power on electron density for H_2 plasma. The effects of deposition parameters on electron density and electron temperature for helium plasma is reported elsewhere [47.] Figure 5.1 shows that electron density is decreasing as the pressure increases. This might be attributed to the increased number of electrons that undergo collisions with neutral species.

Table 5.1 Typical Langmuir data collected at 200W

Pressure (mT)	Electron density (cm^{-3})	Electron temperature (ev)	Plasma Potential (V)
7	1.23E9	5.09	22.87
10	1.2E9	4.3	15.08
15	7.64E8	3.54	12.08
20	4.39E8	2.77	8.76

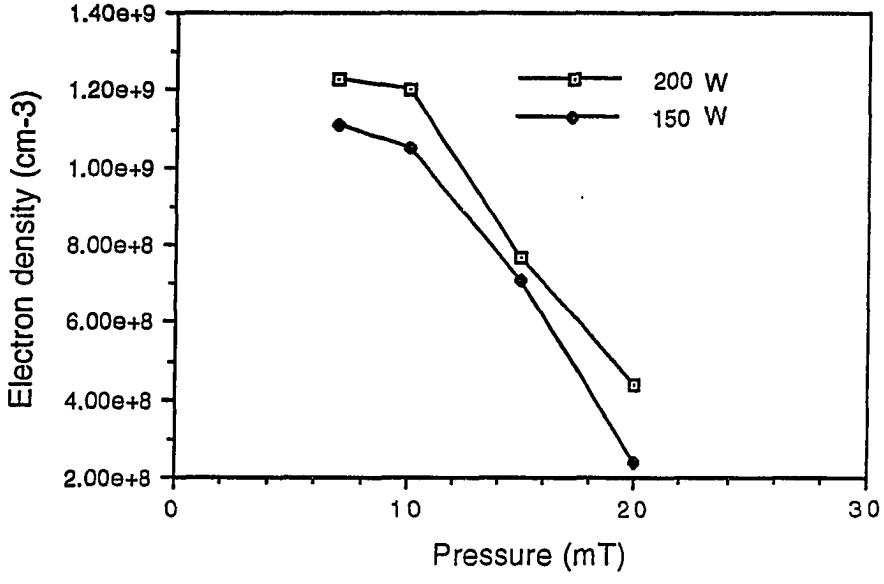

Figure 5.1 Electron density vs. pressure for H_2 Plasma

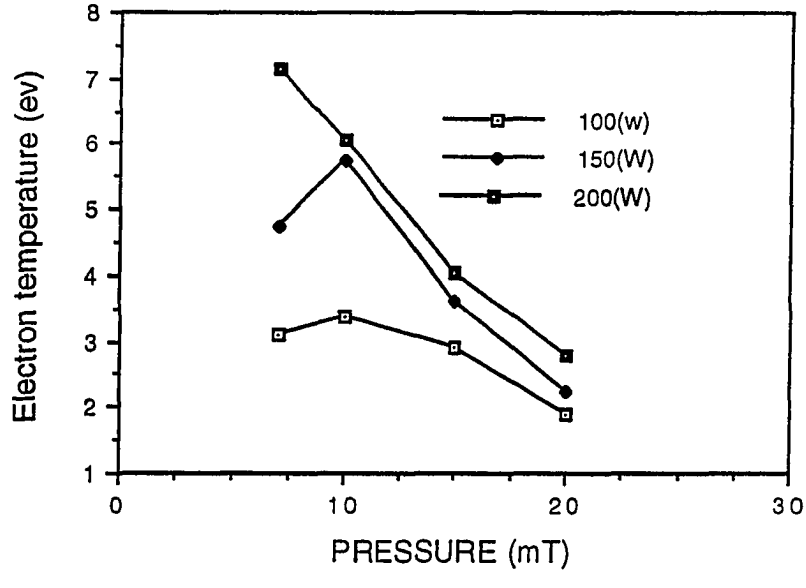

Figure 5.2 Electron temperature for H_2 Plasma

Figure 5.2 depicts the effect of the pressure and power on the electron temperature. The decrease in electron temperature as pressure rises might be due to the increasing number of the collisions that electrons undergo at higher pressures.

2. Optical Emission Spectroscopy

Figure 5.3 shows two peaks corresponding to H^{α} (656nm) and H_2 (610nm). These two peaks provide valuable information regarding the dominant species at the surface of the samples. It is important to note that the

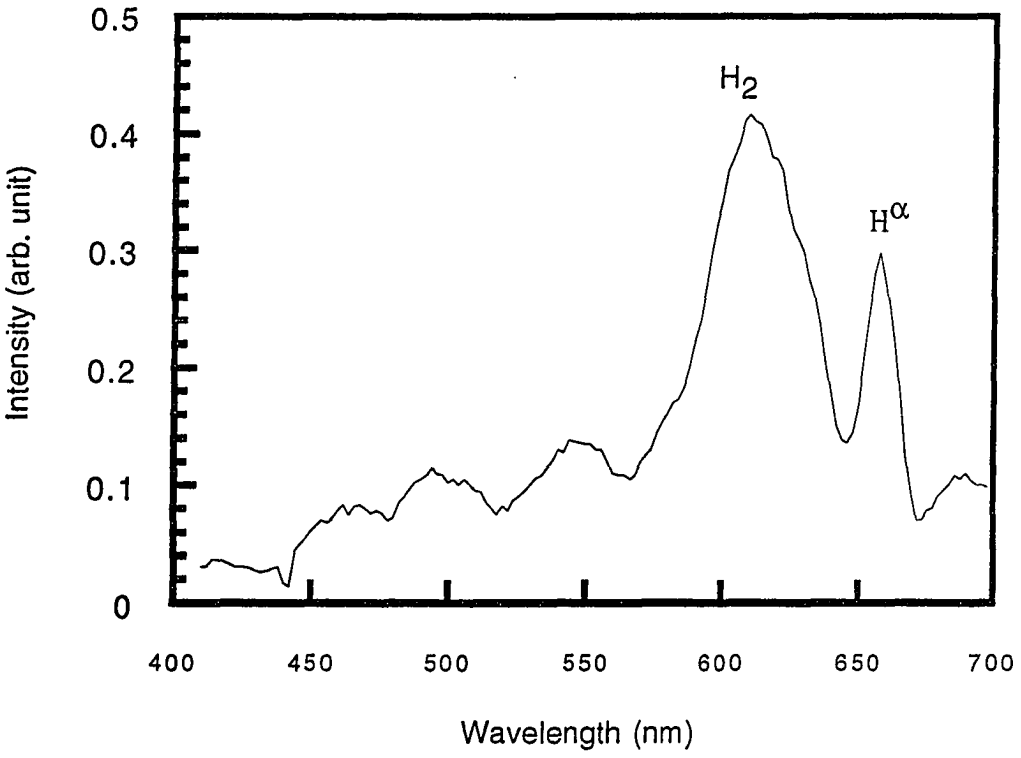

Figure 5.3 H_2 OES spectrum collected at 200W and 5mT

data is collected near the surface of the sample and not in the source, where the hydrogen radicals are generated. In our system hydrogen radicals must travel some distance to reach the substrate. During this transition it is possible that some of the H^{α} recombine and generate H_2 and hence produce a lower H^{α} peak compared to H_2. To examine the effect of the pressure on the hydrogen flux, we monitored the intensity of the emission lines corresponding to H^{α} as a function of the deposition pressure. The result of such a measurement is illustrated in Figure 5.4. This behavior is a consequence of the shorter mean free path at higher pressures.

While most of the investigators have identified the substrate temperature as the main parameter that causes the transition from amorphous to polysilicon, the results of OES indicate that the hydrogen flux plays an important role on the

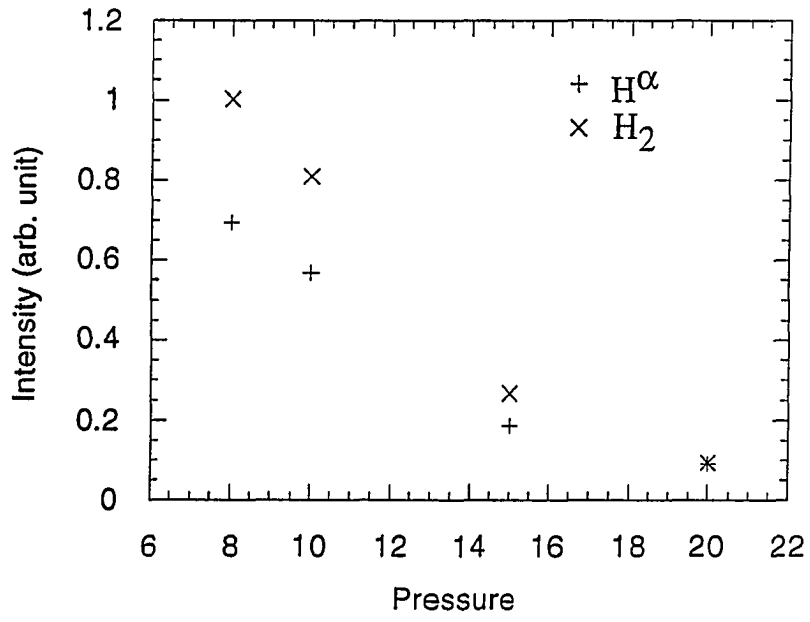

Figure 5.4 OES Spectrum Collect at 200W

film formation and phase transition. This means that by controlling the flux of incoming H radicals it is possible to change the film structure. As expected by lowering the pressure and increasing the mean free path of incoming species, we get polysilicon films. At higher pressures and lower H radicals the deposited films are amorphous.

B. Growth Rate

The growth rate of intrinsic and doped films at different temperatures and deposition conditions was investigated in order to examine the effect of the plasma parameters as well as dopant gasses on the film thickness. The growth rate was calculated by dividing the total thickness by the deposition time. Table 5.1 shows the growth rate versus the deposition temperature. Table 5.1 indicates that the growth rate for RPBE deposited polysilicon films is not sensitive to the deposition temperature. This is understandable because the decomposition of silane gas is governed by the energy of the plasma gas rather

Table 5.1 Growth rate of intrinsic films

Growth rate (Å/min)	Deposition Temperature (°C)
84	400
80	450
85.2	500
87.6	550

than the substrate temperature. This is in contrast to the polysilicon films deposited by LPCVD. Figure 5.5 shows typical growth rate for LPCVD films deposited at 6mT and an incident power of 5W [11].

The growth rate of LPCVD has been characterized in two distinct regimes. At temperatures above 700 ^{o}C the growth rate is constant which means the process gas is depleted near the substrate [11]. This process is known as mass transfer limited reaction. In the case of mass transfer limited reaction, the reaction rate exceeds the rate at which the reactant species arrives at the surface. At temperatures between 600 to 700 ^{o}C the decomposition of silane is limited to pyrolytic effect of the substrate.

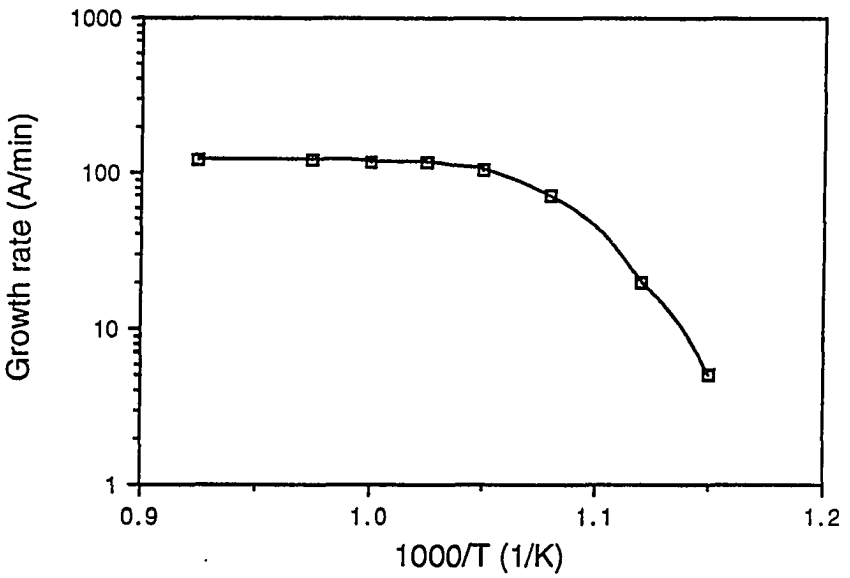

Figure 5.5 Deposition rate for LPCVD polysilicon films Vs. inverse of deposition temperature

Most of the polysilicon films used in integrated circuits are doped and in some applications, such as the gate electrode for MOS devices, the polysilicon films are highly doped. This means that the deposition technique selected for integrated circuits should not be sensitive to the dopant impurities. In the case of LPCVD the in-situ doping, which is a convenient way of adding impurity to the films, has been found to suppress the growth rate significantly [1]. However, for the films deposited by the RPBE, the reduction in growth rate is very small. Figure 5.6 shows the growth rate of the phosphorus doped polysilicon films as a function of the doping rate. The severe reduction of the growth rate in the case of LPCVD has been attributed to the strong absorbance of the phosphorus compared to the silane. This means that phosphorus will block the adsorption of silane by occupying an adsorption site which would have been available for silane. The phosphine molecule has a lonepair electron. This excess valence electron enables it to compete successfully with silane, a fully coordinated molecule, for the available sites. For polysilicon films deposited by LPCVD, the growth rate degrades by a factor of three; whereas for arsine, this can be as high as one order of magnitude [1].

Figure 5.6 shows a little decrease in the growth rate of RPBE deposited as the doping rate is increased from 0.6 sccm to 3.0 sccm. This might be attributed to the high surface mobility and continuos ionic bombardment of the surface that results in a successful competition of reactive radicals with the phosphine for adsorption sites. In other words, the energetic ions break the phosphine monolayer which forbids the growth of the silicon film. We have also used phosphine diluted in argon for growing n type films. The addition of argon makes the growth complicated and as a result the growth rate is degraded by a

factor of two. Moreover the argon atoms have a significant effect on the electrical properties of the grown films, which will be discussed later. The reason for this degradation is not clear, however, it might be due to the absence of additional hydrogen species which can moderate the deposition rate. Very little change in the growth rate was observed as the doping rate was increased from 2 to 5 sccm. Table 5.2 shows the growth rate of the samples doped with PH_3 diluted in argon.

We have also investigated the effect of diborane (B_2H_6) gas on the growth rate. The boron doped films were deposited at temperatures ranging from 400-500 ^oC and the flow rates of hydrogen, silane and diborane were 1, 40 and 6 sccm respectively. The introduction of diborane did not affect the growth rate of the polysilicon films in the range that we investigated. This is in contrast to the LPCVD films, in which by adding diborane, the growth rate increases by a factor of two. The cause of the increase in the growth rate has been explained by the addition of a parallel deposition mechanism to that of undoped polysilicon. For undoped polysilicon, silane decomposes on the surface of the samples. The parallel deposition is thought to be the result of the decomposition of silane on deposited boron surface atoms, which acts as a catalyst [1]. We believe that the parallel deposition mechanism does not apply to the films deposited by plasma enhanced CVD. This is because at the very low pressures that we deposited polysilicon films silane can decomposes very efficiently. This eliminates the possibility for boron atoms to act as a catalyst.

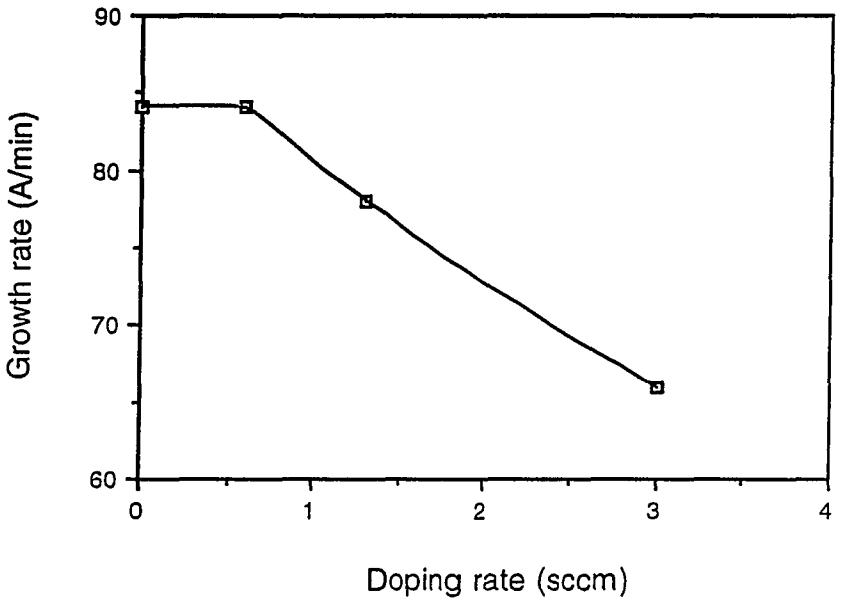

Figure 5.6 Growth rate as a function of doping rate

Table 5.2 Growth rate for samples doped with PH_3 diluted in argon

Growth rate (Å/min)	Doping rate (sccm)
40	1
43.2	3.25
37.2	4
39	5

C. Band Gap

By using the information obtained from the absorbance spectrum, we have calculated the band gap of the deposited films. Figure 5.7 is a graph of square root of the absorption coefficient vs. photon energy. As noted earlier the onset of the square root of the absorption coefficient with the energy determines the band gap.The band gap is estimated based on the assumption that polysilicon film is an indirect band gap material.

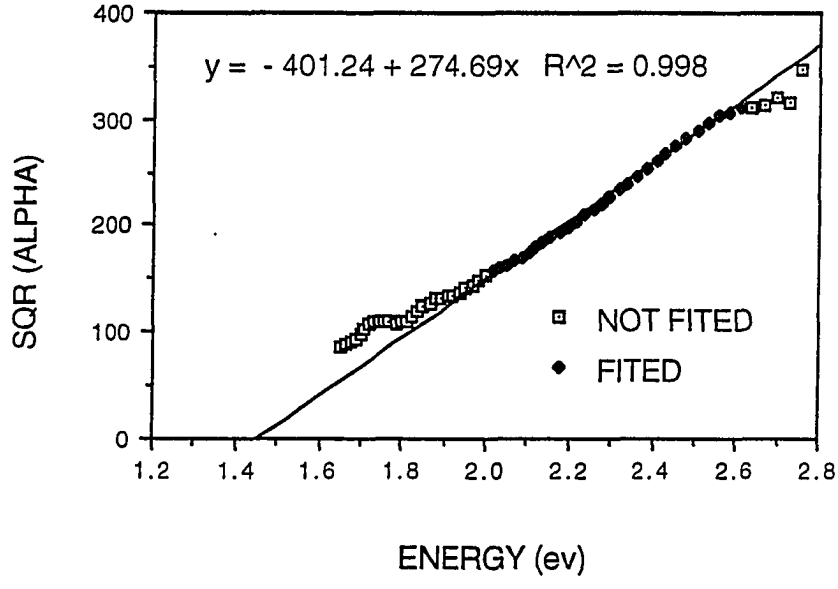

Figure 5.7 Square root of absorption coefficient (alpha) vs. photon energy, sample deposited at 450 ^{o}C other parameters are as described earlier in the text

D. Structural Properties

Several different structural analysis techniques are applied to the grown film. These include UV reflectance, Raman Spectroscopy, and x-ray diffraction. To learn about the crystallinity we have examined all the films by the simple and quick UV reflectance measurement.

1. UV Reflectance

Figure 5.8 illustrates the UV reflectance spectra of crystalline silicon and RPBE deposited amorphous and polysilicon films. As mentioned earlier, the peaks at wave lengths of 280 and 365 nm are related to the interband transition

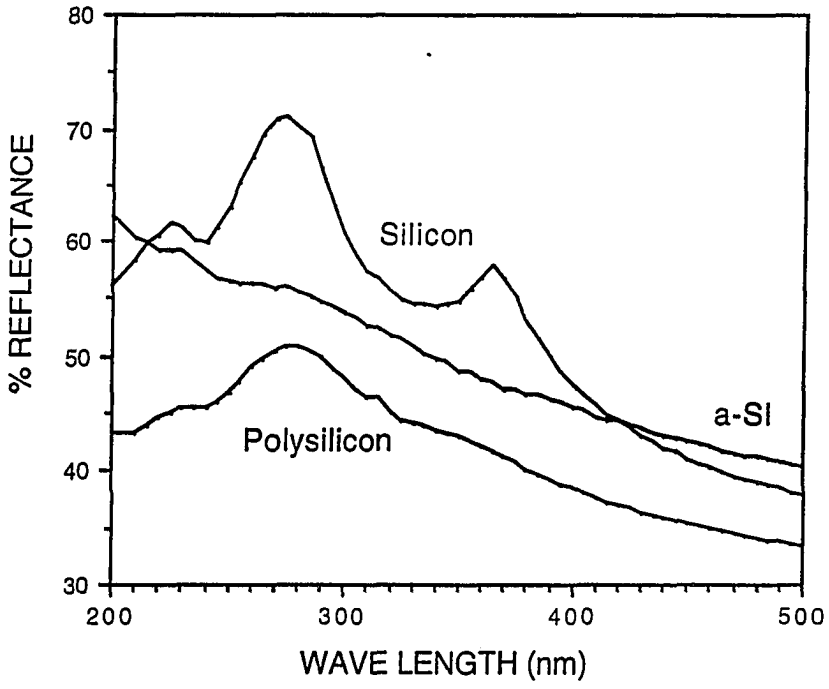

Figure 5.8 Reflectance spectrum of crystalline silicon, amorphous Si and polysilicon

in crystalline silicon. Figure 5.8 shows that these transitions are still valid for polysilicon, while for amorphous silicon where the E-K relation is relaxed these peaks are not present. It is also note worthy that the difference between the reflectance spectrum of the polysilicon and the crystalline silicon increases at lower wave length. This is due to the light scattering which increases with the fourth power of the frequency. Higher reflectance of the amorphous silicon is attributed to smoother surface compared to polysilicon.

2. Raman Spectroscopy

The Raman Spectroscopy technique was applied to several undoped films deposited at different temperatures. Figures 5.9 and 5.10 show the Raman spectrums of the polysilicon films deposited at 400, 450, 500 and 550 ^{o}C. The rest of the deposition parameters are the same as those described earlier. We have also performed Raman spectroscopy on an amorphous film deposited under the same condition but at a pressure of 15mT. The spectrum of the amorphous film is shown in Figure 5.11. Other properties of the amorphous silicon films deposited by the RPBE system and the consideration needed for the design of stable amorphous silicon solar cells can be found in references [27, 48].

The sharp peak at the wave number of approximately of 520 cm^{-1} is attributed to the crystalline silicon, while the broad peak at 480 cm^{-1} has been reported to be a signature of amorphous silicon [36]. This means that the frequency of the phonon is a function of the interatomic force, bond angle and bond length. The origin of the first Raman spectrum in infinite size of crystalline silicon is attributed to the allowed optical phonons at K=0. For a finite

crystalline state transverse, longitudinal and surface modes will contribute to the spectrum, and hence the peak would be broader. For amorphous silicon the K=0 transition is relaxed and the surface mode is dominant, which is in general, lower in frequency than the bulk mode [35]. The asymmetry in the spectrum at the lower wave number is a signature of some degree of disorder in the structure of the deposited films. However the shoulder at about 480 cm^{-1} is much less pronounced compared with the data in current literature. This means that by using RPBE, it is possible to grow polysilicon films with less disorder. For convenience these peaks are tabulated in Table 5.3. The sharp peaks at 520 and 522.5 cm^{-1} indicate that the deposited films are indeed polysilicon.

Table 5.3 Raman peaks of the samples shown in Figures 5.9 -5.11

Sample#	Temperature (^oC)	Raman Peak (cm^{-1})
Amorphous Si	400	474
Polysilicon	400	522.5
Polysilicon	450	520
Polysilicon	500	522.5
Polysilicon	550	520
Silicon	____	521

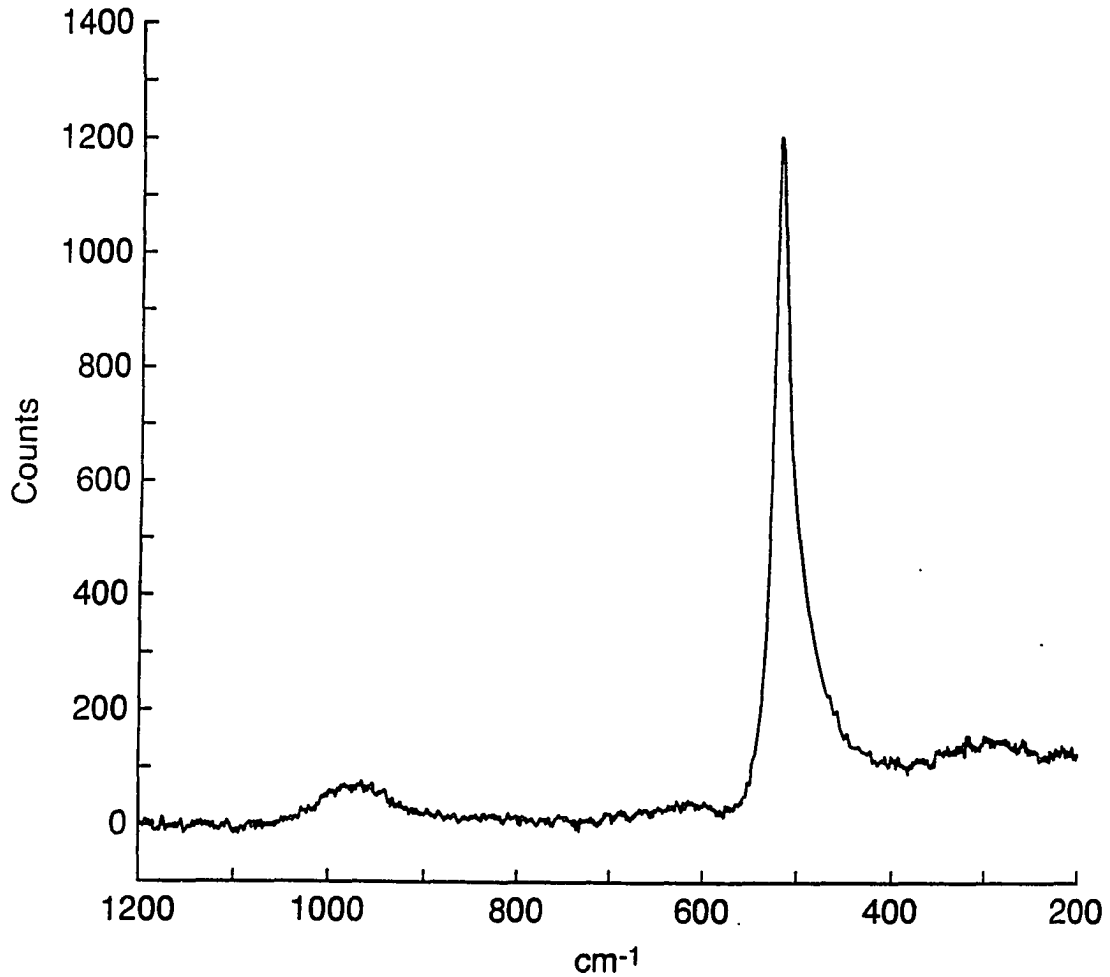

Figure 5.9a Raman spectrum of a typical polysilicon film deposited at 400 ^{o}C

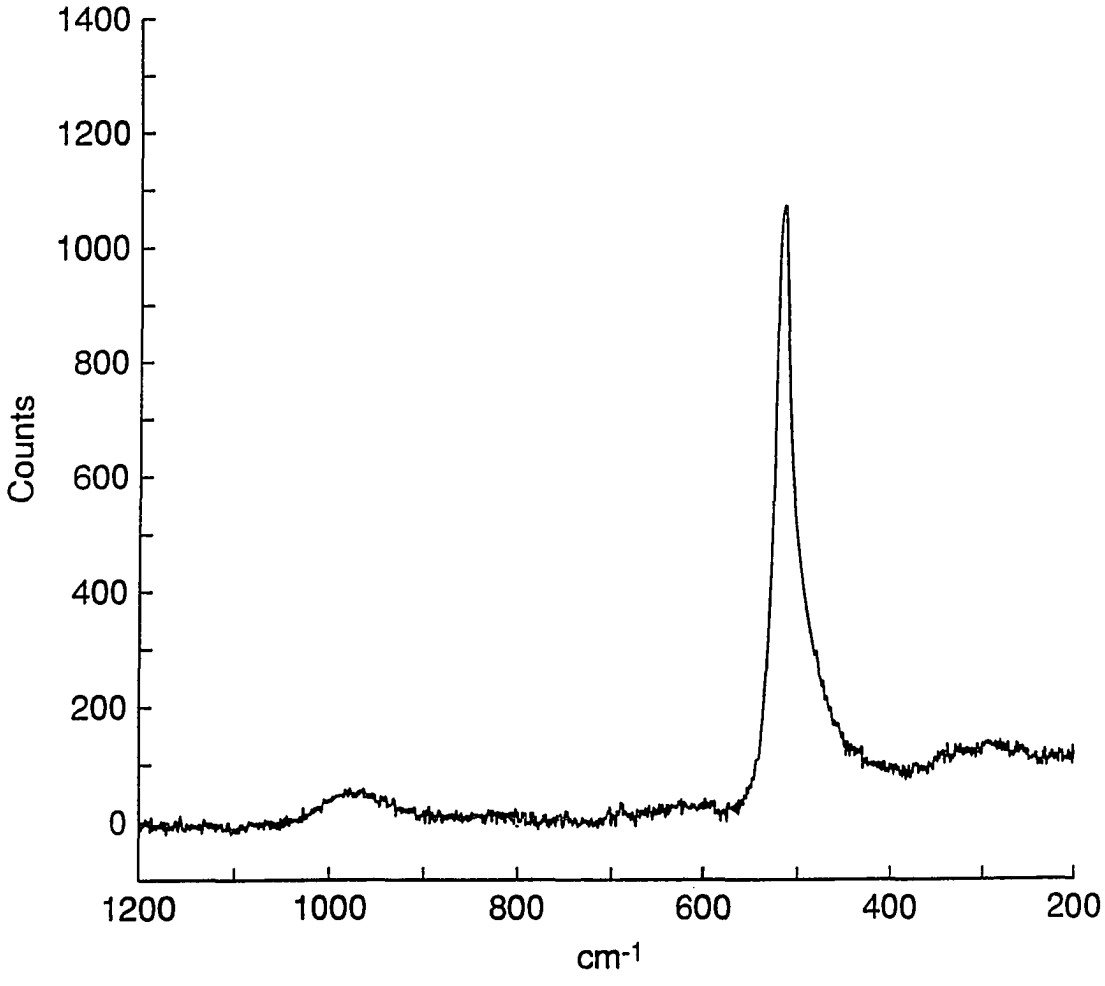

Figure 5.9b Raman spectrum of a typical polysilicon film deposited at 450 °C

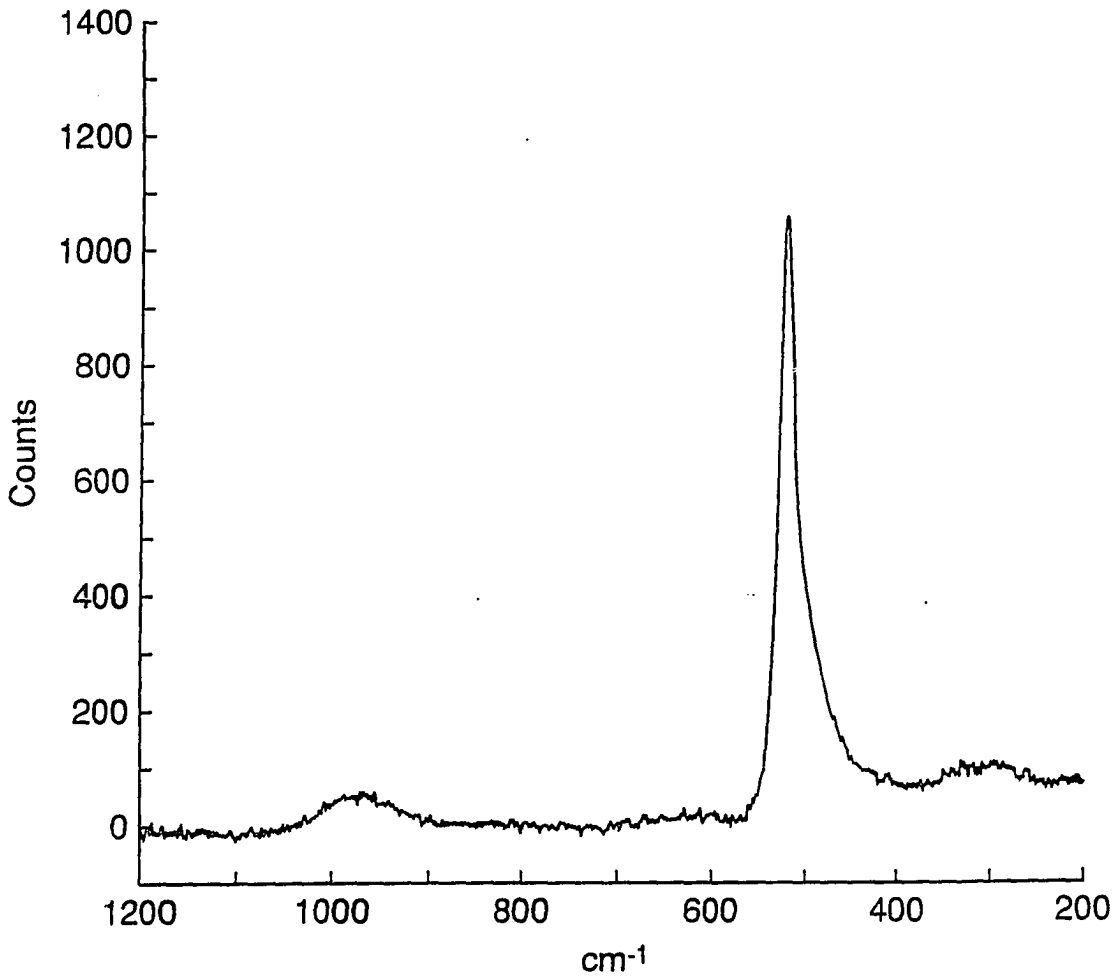

Figure 5.10a Raman spectrum of a typical polysilicon film deposited at 500 °C

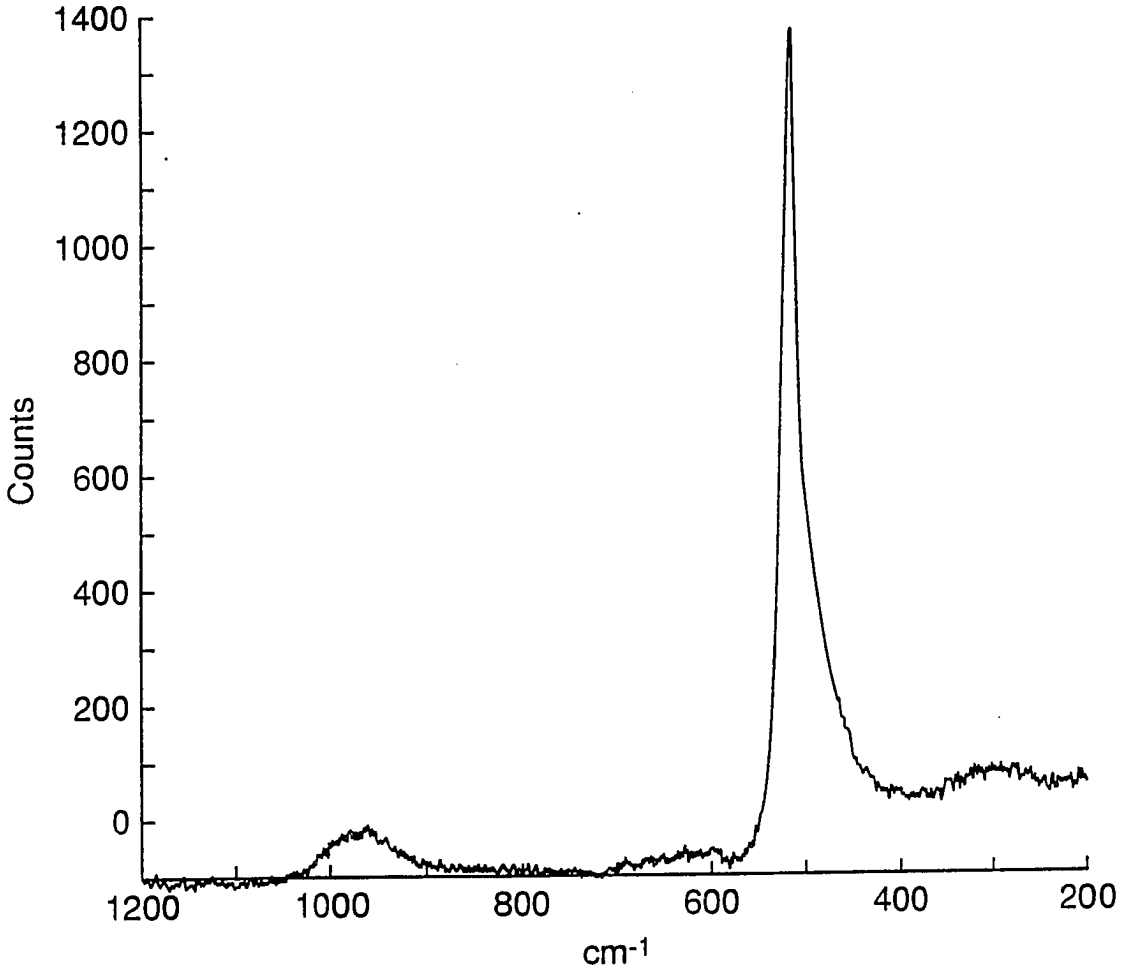

Figure 5.10b Raman spectrum of a typical polysilicon film deposited at 550 °C

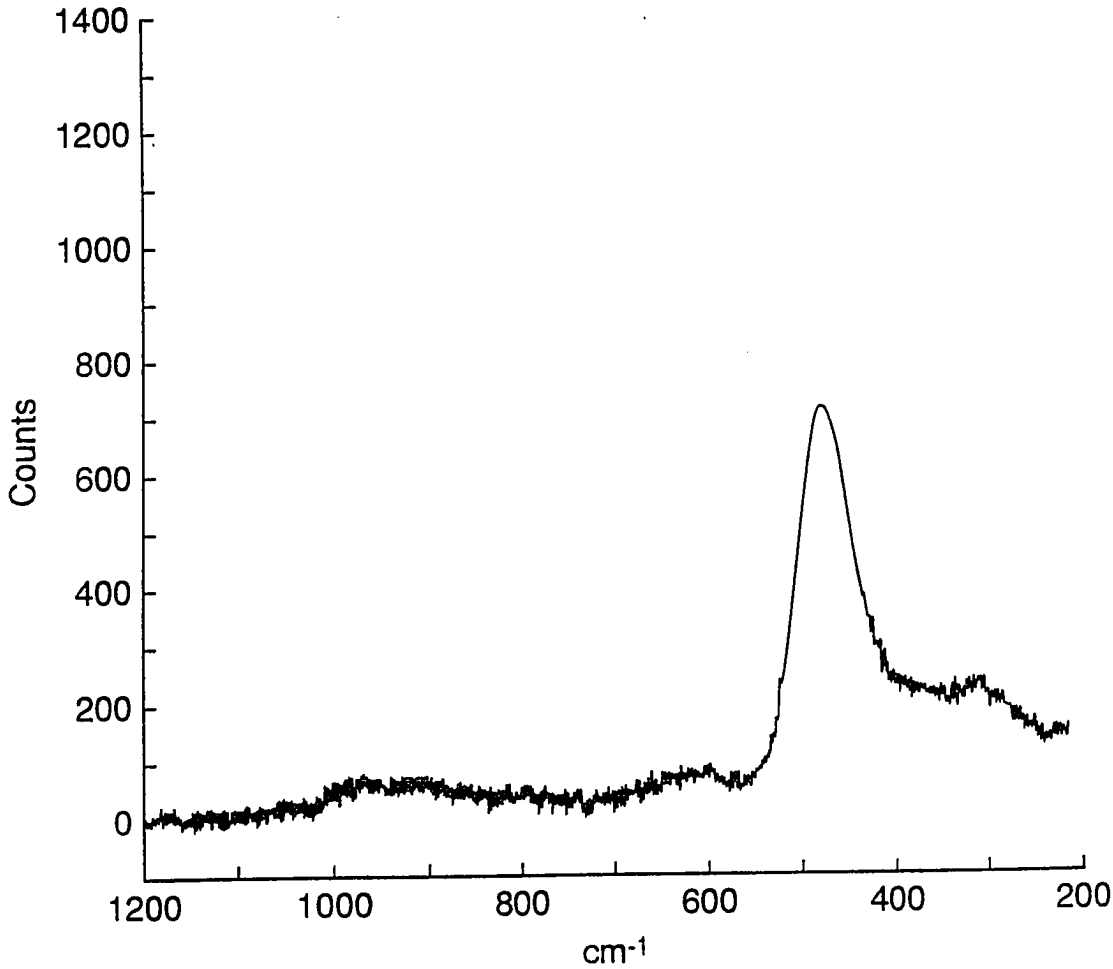

Figure 5.11 Raman spectrum of a typical amorphous silicon film deposited at 400 °C

3. Crystallographic Texture

The texture and the grain size of the intrinsic and the phosphorus doped samples were determined by the means of Read camera and X-ray diffractometer (XRD) techniques. Figure 5.12 depicts the X-ray diffraction of a typical phosphorus doped polysilicon film. Only the peaks corresponding to (111), (220) and (311) planes were detected. Other peaks were not distinguishable from the background noise. The Read pattern is consistent with the XRD showing two intense rings due to (111) and (220) and one weaker ring

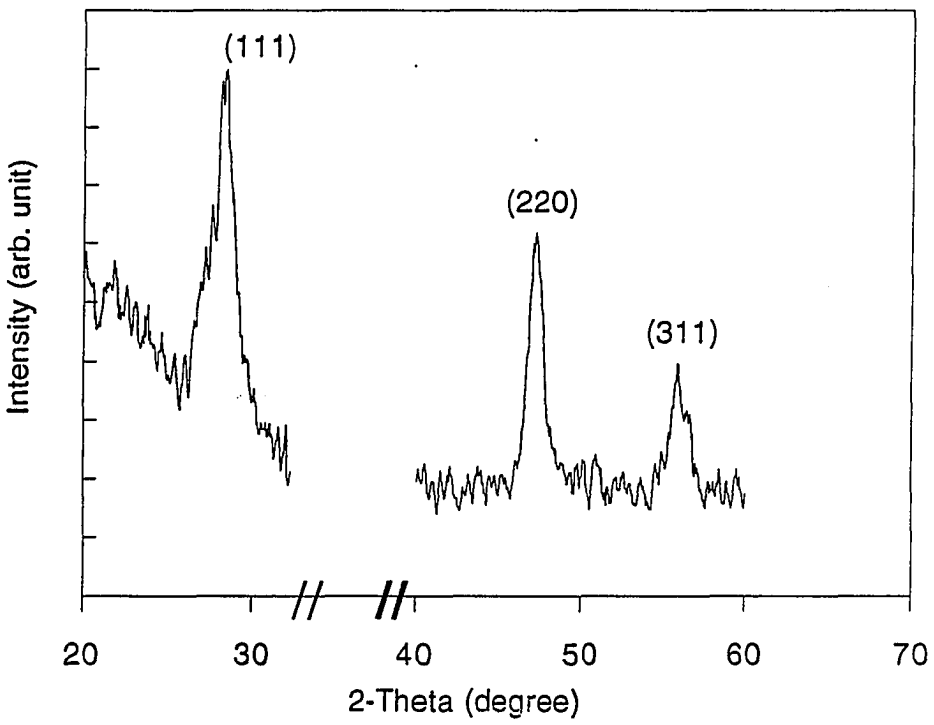

Figure 5.12 XRD of a phosphorus doped polysilicon film

corresponding to (311). Figure 5.13 shows the XRD spectra of a typical polysilicon film deposited at 400 ^{o}C. The XRD spectra of samples deposited at 400 and 450 ^{o}C are shown in Figure 5.14.

The results of XRD measurement indicate that the preferential growth is in the (111) and (220) planes with no significant changes resulting from either the dopants or the temperature. This is in contrast to the data in the current literature[11, 49]. They have reported that (220) is the preferred crystallography orientation of polysilicon films, and correlated the preferred (220) orientation to the surface modification resulting from the reactive hydrogen radicals. They

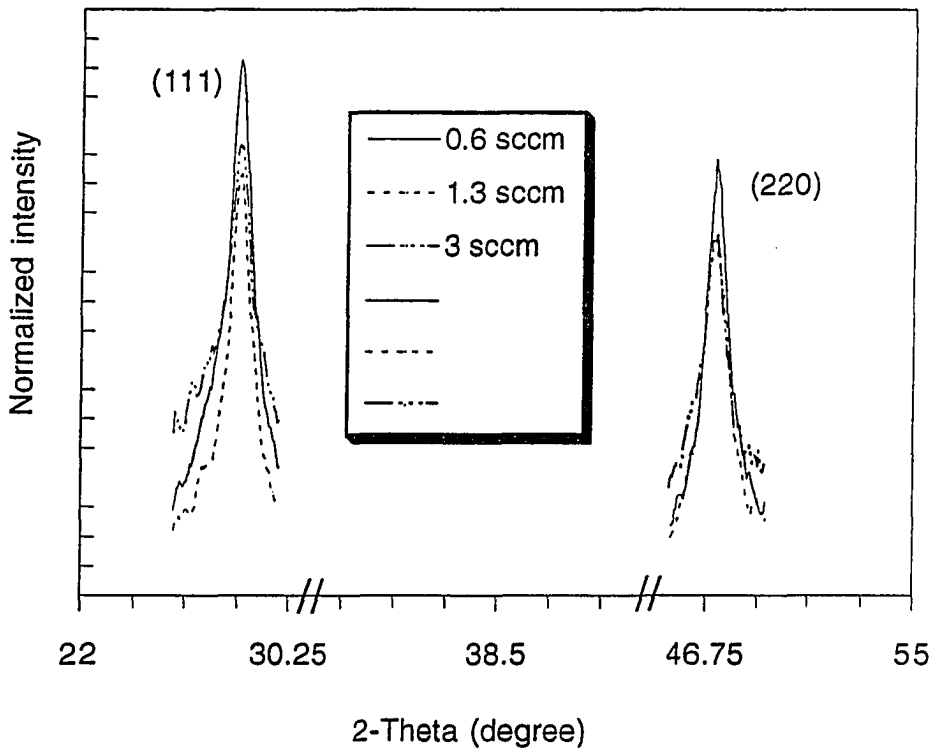

Figure 5.13 XRD spectra for phosphorus doped samples deposited at 400 ^{o}C

believe that the available energy sites which have been created by breaking the Si-O bonds are the main cause for the (220) orientation. Further investigation needs to be done to determine the exact cause of the orientation of (111) and (220) of RPBE films. The XRD spectra of the film deposited on the glass substrate show the same orientation as the films deposited on SiO_2.

4. Grain Size

Table 5.4 shows the grain size of the intrinsic and doped polysilicon films deposited at 400 ^{o}C. The effect of the temperature on the grain growth of polysilicon films deposited on SiO_2 is shown in Table 5.5. For the range we

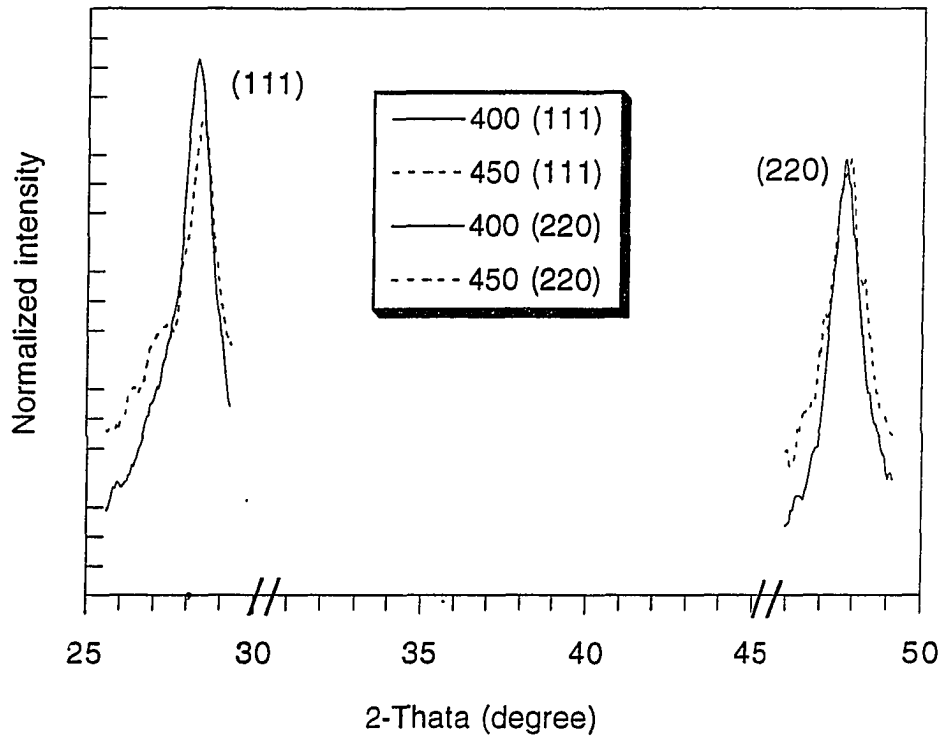

Figure 5.14 XRD spectra for the polysilicon films deposited at 400 and 450 ^{o}C

investigated the grain size is not sensitive to the dopant concentration and the type of substrate. However, a small increase in the grain size at higher temperatures was observed. This can be attributed to the higher surface mobility which decreases the number of the nuclei. The fine grain size might be

Table 5.4 Grain size of polysilicon film deposited at 400 ^{o}C

Substrate	Grain size (Å)		Average size (Å)	Dopant rate
	(111)	(220)		(sccm)
Glass	122	143	132	___
SiO_2	113	157	135	0.6
SiO_2	116	102	109	1.2
SiO_2	129	113	121	3.0

Table 5.5 Grain size of polysilicon films deposited at different temperatures

Temperature	Grain size (Å)		Average size (Å)
(^{o}C)	(111)	(220)	
400	113	157	135
450	205	157	181
500	136	245	190

explained in terms of higher absorption of the process gases. As mentioned earlier, the size of the critical cluster is a strong function of the arrival rate and the desorption rate. As the rate of the incoming process gas increases the density of nuclei will also increase and results in smaller grain size.

E. Surface Morphology

The surface morphology of the polysilicon films has been studied by using the UV reflectance spectrum and the scanning electron microscope techniques. The UV spectrum of the polysilicon film was used to quantify the effect of the temperature and doping concentration on the surface roughness of the deposited films. Qualitative information about the surface morphology was obtained by using an SEM.

1. Surface Roughness

UV reflectance measurements were used to estimate the surface roughness of the deposited films. From such a measurement, the root mean square (RMS) value of the surface roughness can be calculated. Figure 5.15 shows the square root of $\log(R_{Si}/R_{poly})$ as a function of inverse wavelength for a polysilicon film deposited at 400 ^{o}C. The slope of such a curve can be used to determine the RMS value of the surface roughness.

Table 5.6 shows the RMS value of the surface roughness (σ) for the polysilicon films deposited on 7059 glass substrates at a deposition temperature of 400 ^{o}C. The RMS value of surface roughness as a function of temperature is shown is Table 5.7. The value of surface roughness for the

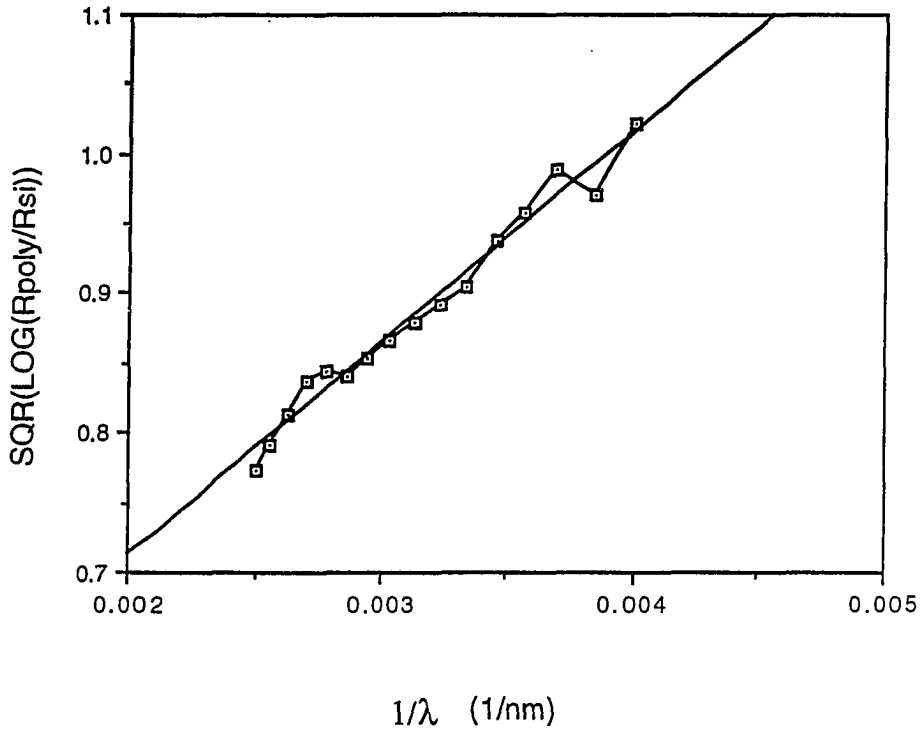

Figure 5.15 Square root of log(Ro/R) vs. inverse wave length

Table 5.6 Surface roughness of a typical polysilicon film deposited at 400 ^{o}C

σ (Å)	doping rate sccm
124	———
123	0.6
126	1.3
160	3

Table 5.7 RMS value of surface roughness for different temperatures

Temperature (°C)	σ (Å)
400	124
450	164
500	180
550	167

samples deposited on SiO_2 substrates is smaller approximately by a factor of two. The surface roughness of the samples deposited by RPBE is quite low and it does not change significantly as the doping concentration increases from 0.6 to 3 sccm. The insensitivity of the surface roughness to the doping concentration is very important in integrated circuits where highly doped polysilicon films are used for the gate electrodes.

2. Scanning Electron Microscopy Technique

The scanning electron microscope (SEM) was used to examine the effect of the deposition parameters on the surface morphology of the polysilicon films. Because of the absence of surface features in polysilicon films and the high density of the grains, SEM does not provide a significant amount of information regarding the effect of the plasma parameters on the structure and morphology of the films. As discussed earlier the deposition temperature and

the doping concentration did not have a significant effect on the surface morphology of the RPBE samples. Therefore, the SEM microghraphs of polysllicon films in this investigation were basically the same. However, it is possible to use the SEM to compare the smoother surface of amorphous films with rough polysilicon films. Such a comparison is shown in Figure 5.16. The surface roughness obtained from this technique is, in general, higher by a factor of five compared to UV reflectance measurements.

F. Doping Concentration

The chemical constituents of the deposited films were determined by secondary ion mass spectroscopy (SIMS). Figure 5.17 shows the depth profile of a typical phosphorus doped polysilicon film deposited on a silicon substrate. Figure 5.18 is the depth profile for a polysilicon sample deposited on a silicon dioxide substrate. A summary of the experimental conditions under which the SIMS measurement was performed as well as depth profiles of other samples can be found in appendix C.

The SIMS results show that the distribution of hydrogen is reasonably homogenous at a concentration of about $1x10^{21}$ atom/cm^3 in all the samples. The oxygen increases significantly midway into the polysilicon layer on the samples deposited on silicon dioxide. Carbon concentration fluctuates in the range of $1\text{-}5x10^{19}/cm^3$. The phosphorus concentration of the samples investigated varied from $3x10^{18}$ to $3x10^{20}/cm^3$. Table 5.8 shows the doping concentration and phosphine flow rates for these samples. For sample 308, 1% PH_3 diluted in H_2 was used. Samples 589 and 590 were doped by using 100 ppm PH_3 diluted in hydrogen.

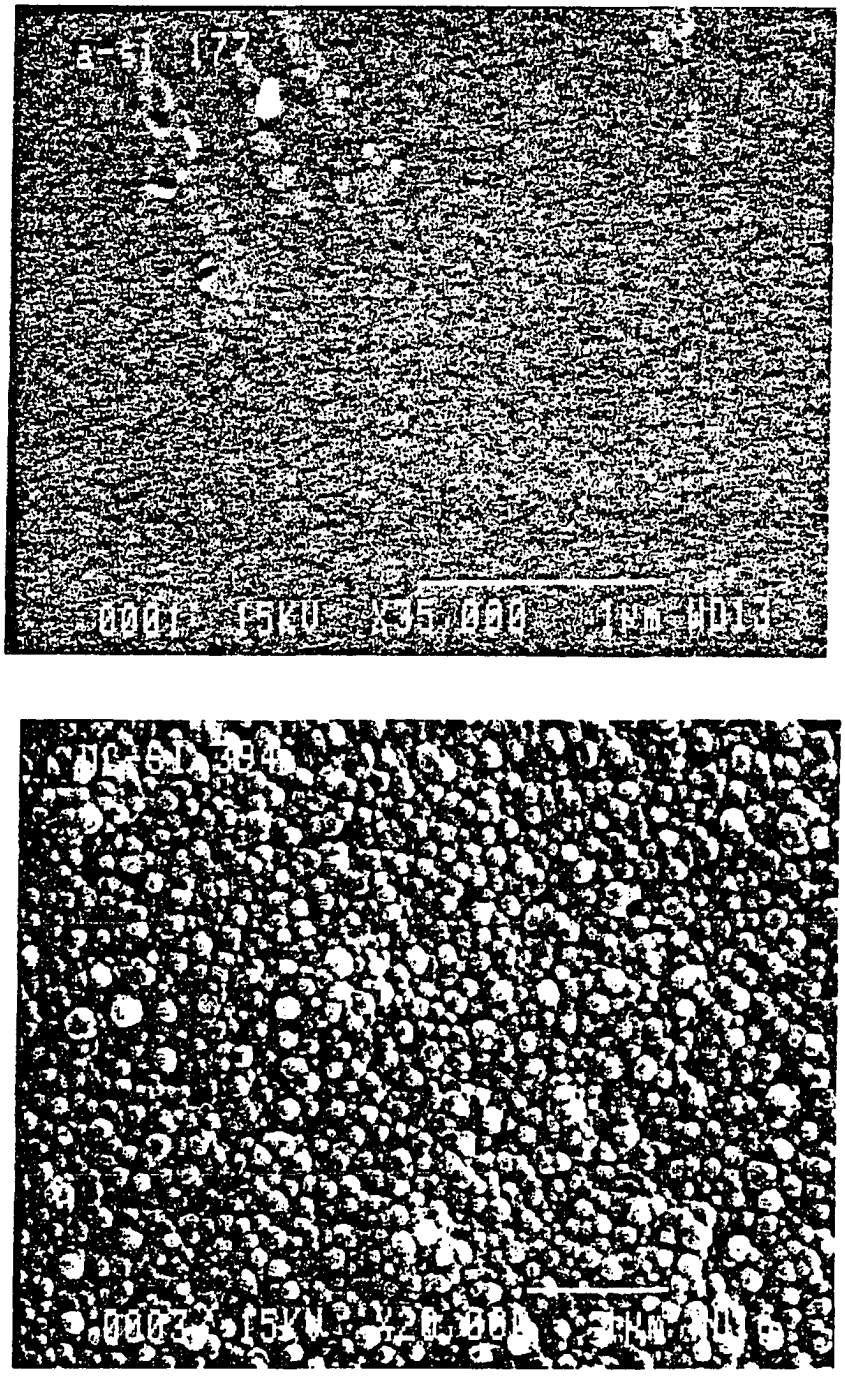

Figure 5.16 SEM micrograph of a) amorphous silicon, b) polysilicon

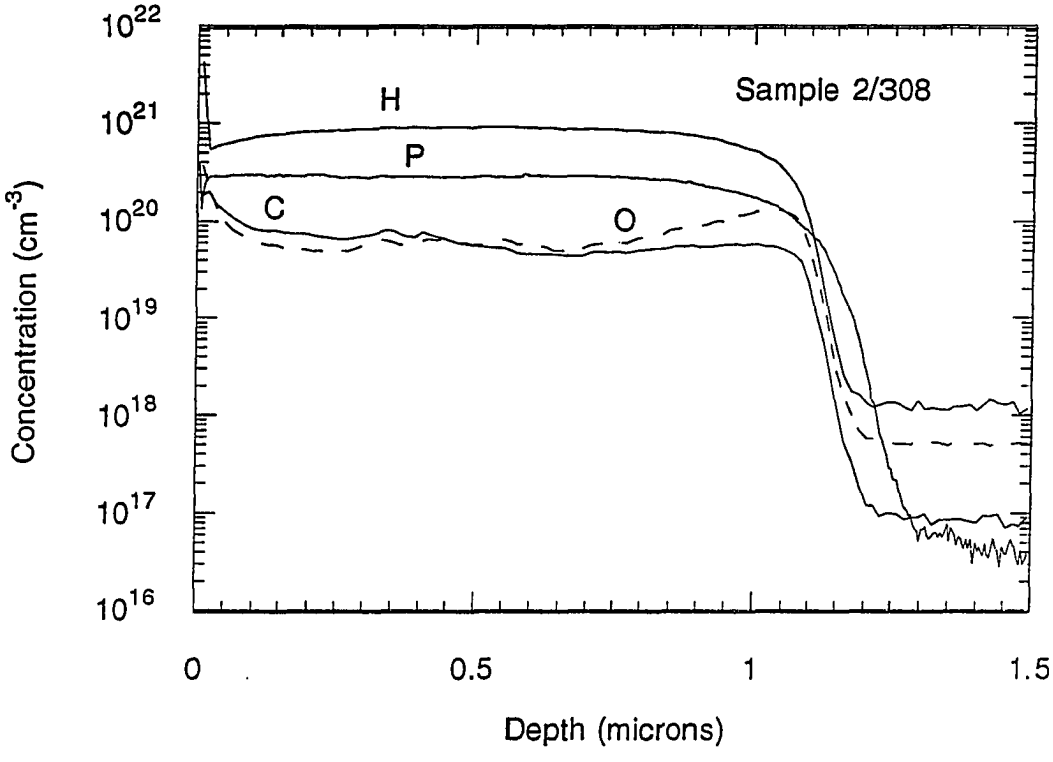

Figure 5.17 SIMS Profile of a typical polysilicon sample deposited on silicon substrate

Table 5.8 SIMS results of the phosphorus doped samples

Sample#	flow rate (sccm)	doping conce. (cm^{-3})	substrate
589	1.3	$3x10^{18}$	SiO_2
590	3	$5x10^{18}$	SiO_2
308	7	$3x10^{20}$	Si

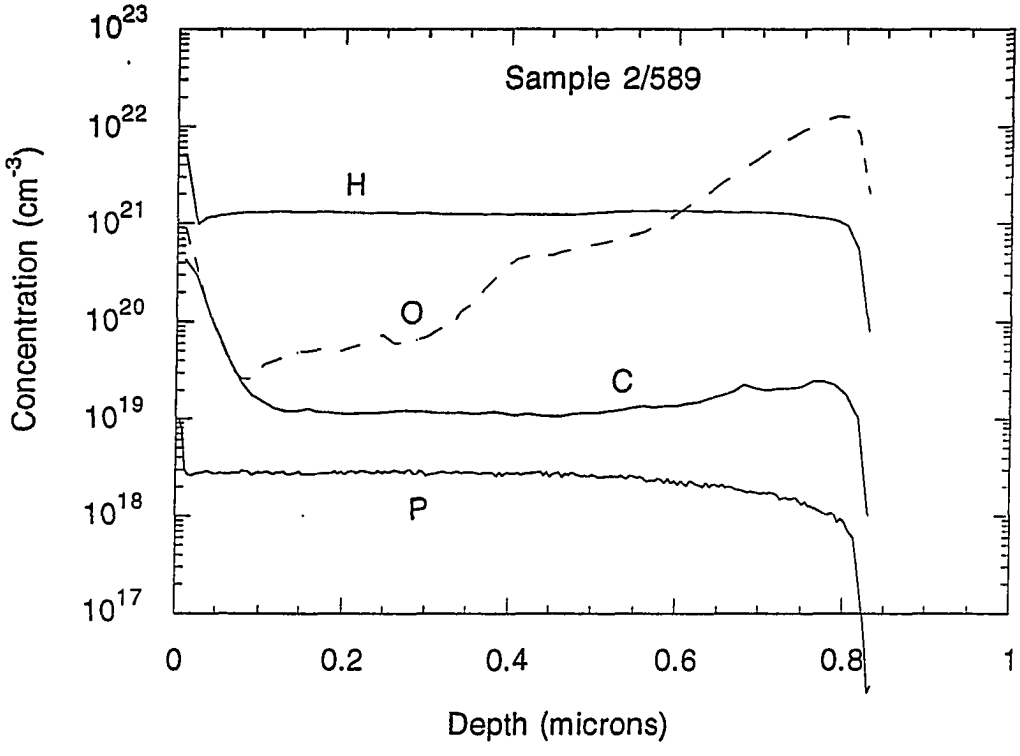

Figure 5.18 SIMS profile of a typical polysilicon sample deposited on a SiO_2 substrate

G. Electrical Characterizations

Electrical properties of the deposited polysilicon films were investigated by the means of conductivity, mobility and activation energy measurements.

1. Conductivity

To examine the transport mechanism of polysilicon films, the conductivity of the deposited films was measured as a function of temperature. Figure 5.19

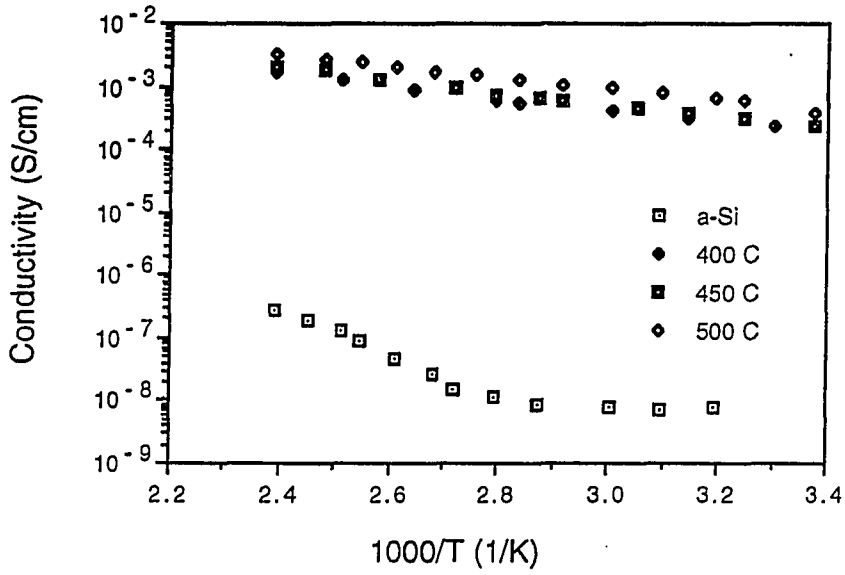

Figure 5.19 Conductivity vs. inverse temperature

illustrates the result of such measurements. At a deposition pressure of 6-7 mT the films show similar conductivity behavior in the range that we investigated. However as pressure increases from 7mT to 15mT the conductivity of the films decreases significantly and the behavior of the conductivity vs. temperature changes dramatically.

The films deposited at 6-7mT exhibit a single activation energy which indicates that the conduction occurs via extended states [50]. The conductivity vs. inverse temperature of the film deposited at 15mT (a-Si) can be divided into two regions: one at high temperatures and another at low temperatures. This behavior indicates the presence of two conduction mechanisms, a high activated process at high temperatures and a less activated process at lower temperatures. The conduction at lower temperatures is due to the contribution

of the electrons trapped in the mid gap which hop from one localized state to another at low temperature[10]. The temperature dependence of conduction via mid gap states is estimated to be inversely proportional to the fourth power of the temperature [51].

The results of introducing PH_3 diluted in hydrogen on conductivity of the films deposited on glass substrates are summarized in Table 5.9. The conductivity of these films has increased by two orders of magnitude compared

Table 5. 9 Conductivity of polysilicon films deposited on 7059 glass substrates (deposition pressure 7mT)

Temperature (^oC)	doping rate (Sccm)	Conductivity (S/cm)
400	_	1.6e-4
400	0.6	3.2e-2
400	3	6.3e-2
450	__	1.76e-4
450	0.6	3.3e-2
450	1.2	5.6e-2
450	3	6.7e-2
500	__	3.8e-4
500	0.6	3.59e-2
500	1.2	7.7e-2

to intrinsic films. The higher conductivity of the intrinsic film deposited at 500 ^{o}C is due to the lower deposition pressure (6 mT) of this particular sample. The conductivity of the samples deposited on silicon dioxide substrates is about one order of magnitude higher compared to the films deposited on glass substrates. This can be attributed to the larger grain size of the films deposited on silicon dioxide. Figure 5.20 illustrates the effect of deposition temperature and doping rate on films deposited on silicon dioxide substrates.

Moreover, the conductivity of the films that were doped with the PH_3 diluted in argon was also measured and found to be about one order of magnitude lower than the conductivity of the films prepared by using phosphine

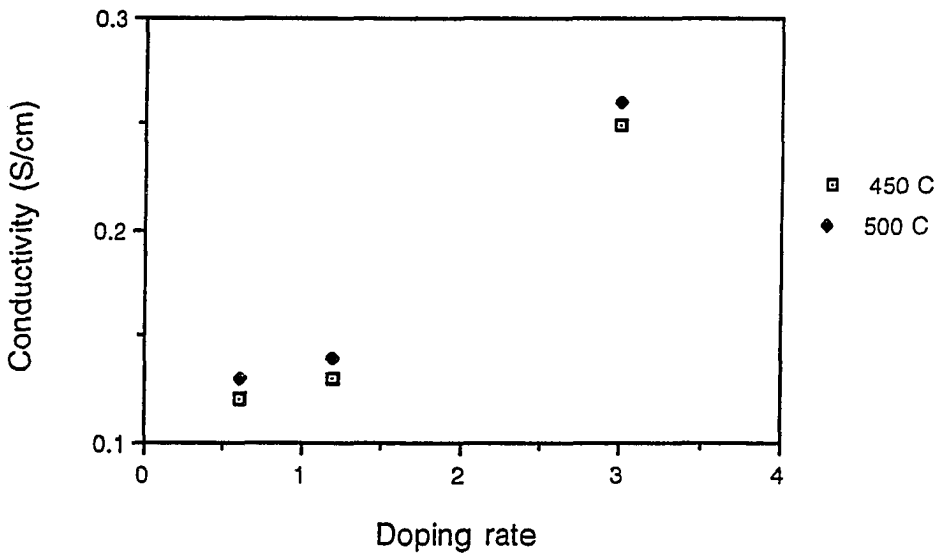

Figure 5.20 Conductivity of the n-type polysilicon deposited on SiO_2 substrates

diluted in hydrogen. The conductivities and the doping rate of these films are summarized in Table 5.10. The lower conductivities of these films might be due to the absence of additional hydrogen species which moderate the deposition rate and improve the nucleation.

We have also examined the effect of diborane on the conductivity of the polysilicon films. The results of the conductivity measurement of boron doped films are summarized in Table 5.11. The conductivity of the p-type samples is lower one order of magnitude compared to the intrinsic films. This is probably due to the compensation of the donor defects such as oxygen. This is also an indication that the intrinsic films are slightly n type.

2. Activation Energy

The activation energy of the deposited films was estimated from the slope of the Arrhenius plot obtained from the logarithm of conductivity vs

Table 5.10 Conductivity of n-type polysilicon films prepared by using PH_3 diluted in argon and at a deposition temperature of 450 ^oC

Conductivity (s/cm)	doping rate (Sccm)
$1.06x10^{-3}$	2
$6.09x10^{-3}$	3.5
$7.14x10^{-3}$	4
$1.28x10^{-2}$	5

inverse temperature. The activation energies of the intrinsic films are shown in Table 5.12. The activation energies of the n-type samples varied from 0.17 to 0.06 eV as the doping rate changes from 0.6 to 3 Sccm. For p-type samples the activation energy was 0.3 eV.

Table 5.11 Conductivity of p-type films

Temperature (°C)	Conductivity (S/cm)
400	1.98×10^{-5}
450	2.05×10^{-5}
500	2.37×10^{-5}

Table 5.12 Activation energy of the polysilicon films

Deposition Temp. (°C)	Activation energy (eV)
400	0.18
450	0.19
500	0.21

3. Hall Mobility

Hall mobility measurement was carried out on samples deposited on silicon and silicon dioxide substrates. Highly doped polysilicon films prepared on silicon substrates at temperatures as low as 500 ^{o}C have electron mobility as high as 40 $cm^2/V.S$. We should emphasize that such a large mobility was obtained without post deposition annealing. The average carrier concentration obtained from Hall mobility measurement for highly doped samples is $1x10^{20}/cm^3$. Due to the high resistivity of the moderately doped polysilicon films, changes in the Hall voltage as a function of magnetic field were usually below the noise level of the instrument. Thus, the Hall mobility measurement in this range might not be accurate. However the Hall mobility of the lightly doped samples that we were able to measure were in the range of 12 to 35 $cm^2/V.S$

Table 5.13 Doping concentration, carrier concentration and mobility of typical phosphorus doped samples

Sample#	Doping concen. (cm^{-3})	Carrier Con. (cm^{-3})	Mobility ($cm^2/V.S$)	Conductivity (S/cm)
589	$3x10^{18}$	$3x10^{16}$	25	0.13
590	$5x10^{18}$	$5x10^{16}$	33	0.26
308	$3x10^{20}$	$1x10^{20}$	40	640

for the doping rate ranging from 0.6 to 3 sccm. The carrier concentration of these samples was in the range of 1e16 to 4e16. Table 5.13 shows the carrier concentration and the mobility for three samples with different doping concentration.

The behavior of the mobility as a function of doping concentration in polysilicon films is opposite to that of crystalline silicon. In the case of crystalline silicon the mobility is not sensitive to the carrier concentration in the low to moderately doped regimes, while at higher carrier concentration the presence of the ionized impurities significantly suppress the mobility. For polysilicon films the behavior of mobility is very much controlled by barrier height as discussed earlier.

We have also measured the Hall mobility of polysilicon films as a function of temperature. Figure 5.21 shows the result of such a measurement. The behavior of mobility as a function of temperature of polysilicon films is in contrast to crystalline silicon. It is well known that in the crystalline silicon the mobility decreases as the temperature increases. Such a behavior is attributed to the lattice vibration and other scattering mechanisms [22]. In the case of polysilicon as the temperature increases the carriers gain more energy, and hence they can overcome the barrier height more easily. The slope of the mobility vs. inverse temperature can be used to estimate the barrier height of the polysilicon films.

To compare experimental results with theoretical values E_b and grain size must be known. The grain size was calculated from the Scherrer's formula as explained in chapter three. E_b was estimated from the slope of mobility vs. temperature. Table 5.14 shows the barrier height and theoretical and

experimental values of mobility for three samples with different doping concentration.

Table 5.14 Barrier height and mobility for three samples with different doping concentration

Doping Con. (cm^{-3})	Barrier height (ev)	Mobility ($cm^2/V.S$)	
		Theory	Experiment
$1x10^{18}$	0.05	23	25
$3x10^{18}$	0.045	28	33
$3x10^{20}$	0.034	42	40

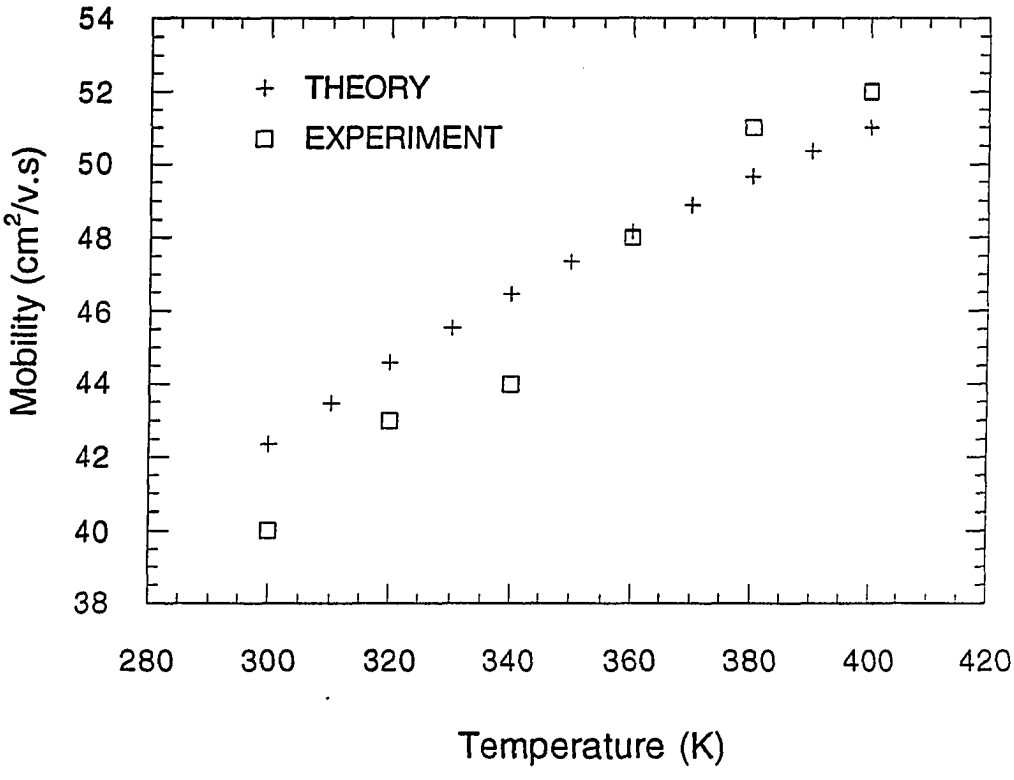

Figure 5.21 Electron mobility as a function of temperature

VI. CONCLUSIONS

Intrinsic and doped polycrystalline silicon were deposited by reactive plasma beam epitaxy techniques. Langmuir probe and optical emission spectroscopy were used to study the behavior of the plasma as the pressure and the power were changed. A number of characterization techniques were used to analyze the structural, compositional, optical and electrical properties of the films.

The results of Langmuir probe indicate that higher electron density and electron temperature can be obtained at lower pressures. Electron density was always found to be larger for the magnet optimized plasma compared to tuner optimized plasma. The smaller electron density and electron temperature at higher pressures were attributed to the increased number of the collisions that electrons under go with neutral species.

Optical emission spectroscopy was used to monitor the intensity of the hydrogen and silane optical transitions. Two peaks at (656nm) and (610nm) corresponding to H^{α} and H_2 were detected for hydrogen plasma. The effect of the pressure on the flux of incoming H radicals in the deposition chamber was examined by monitoring the intensity of the emission lines corresponding to H^{α}. The results of such a measurement showed stronger intensity at lower pressures. The stronger intensity at the lower pressures might be attributed to the large mean free path of the H radicals which results in less recombination.

The growth rate of the intrinsic and doped films at different deposition conditions were investigated in order to examine the influence of the plasma as well as the dopant gases. For intrinsic films the growth rate was about 85Å/min and showed no sensitivity to the deposition temperatures. The effect of

phosphine and diborane diluted in hydrogen was also found to be insignificant. However, the growth rate of the n-type samples diluted in argon was lower by a factor of two.

Raman spectroscopy was used to verify the polycrystallinity nature of the samples. The Raman spectra of the polysilicon films deposited at 400-550 ^{o}C were basically the same with a sharp peak at about 520 cm^{-1}. Moreover, the results of the Raman spectroscopy revealed that films deposited at the pressures of 6-7mT were polysilicon, while those deposited at higher pressures (i.e. 15-20mT) were amorphous.

X-ray diffraction was used to identify the crystallography orientation as well as the grain size of the polysilicon films. The results of the x-ray diffraction indicate the orientation in the (111), (220) and (311) planes. The grain size estimated form Scherrer formula was in the order of 200Å. For the parameters used in this research investigation, the grain size was found to be insensitive to both the doping concentration and the substrate type. The small grain size was attributed to higher absorption of the process gas which results in a larger number of the nuclei. The small increase in the grain size at higher temperatures was attributed to the higher surface mobility.

The surface morphology of the polysilicon films was investigated by the means of optical measurements and SEM. The UV reflectance was used to estimate the surface roughness of the samples. The RMS value of the surface roughness determined by this method was found to be small compared with the data in current literature, and showed little change as the to the doping concentration and temperature were varied.

Electronic properties of the deposited films were characterized by

measuring the conductivity, Hall mobility and activation energy. The conductivity and activation energy of the intrinsic films deposited at 400 ^{o}C were $1.6X10^{-4}$ and 0.18eV respectively. Higher deposition temperatures did not affect the conductivity significantly. However the activation energy was increased form 0.18 to 0.21 as the deposition temperature was increased form 400 to 550 ^{o}C. The introduction of PH_3 diluted in hydrogen increases the conductivity of these films by two to three orders of magnitude. The conductivity of the films that were doped with PH_3 diluted in argon was also measured and found to be about one order of magnitude lower than the conductivity of the films prepared by using PH_3 diluted in hydrogen. The lower conductivity of these films might be due to the absence of additional hydrogen species which moderate the deposition rate and improve the nucleation. The conductivity of the p-type samples is lower by one order of magnitude compared to the intrinsic films. This is probably due to the compensation of the donor defects such as oxygen, and also indicate that the intrinsic films are slightly n type.

To examine the transport mechanism of polysilicon films, the conductivity of the deposited films was measured as a function of temperature. The films deposited at 6-7mT exhibit a single activation energy, which indicates that the conduction occurs via extended states. While films deposited at 15mT (a-Si) show two distinct regions. One at high temperature and the other at low temperature. The conduction at lower temperature was attributed to the contribution of the electrons trapped in the mid gap states which hop from one localized state to another. The transition from amorphous to polysilicon at lower pressures might be attributed to the larger mean free path of the plasma gas which results in less recombination of H radicals and consequently more

effective etching of weak Si-Si bonds (amorphous Si) during the growth.

Hall mobility measurements were carried out on samples deposited on silicon and silicon dioxide substrates. Highly phosphorus doped samples have mobolities of 40 $cm^2/v.s$. Lightly doped polysilicon films deposited on the silicon dioxide substrates have mobilities ranging form 12 to 30 $cm^2/v.s$. These mobilities were obtained without any post deposition annealing.

Although the results of this research investigation show the possibility of deposition of polysilicon with high mobility and reasonable surface roughness, it would be premature to conclude that RPBE deposited films can meet all the challenges of the integrated circuit technology. Moreover, the materials presented in this dissertation is based on the film characterizations. Therefore, it is essential to make devices such as polysilicon diodes and MOS structures to examine the performance of the RPBE deposited films. Surface roughness of the films must be greatly improved in order to be able to perform submicron lithography on these films.

REFERENCES

[1] Kamin, Ted, Polysilicon for Integrated Circuits, Kluwer Academic Press, Boston, 1988.

[2] Mandurah, M., Sarawt, K. C., Kamin, Ted, IEEE Transactions on Electron Devices, Vol., ED, No. 10, P. 1163, 1981.

[3] Hammound, M., in Polysilicon Thin Films and Interfaces, edited by T. Kamin, B. Raicu, C. V. Thomson, Material Research Society Symposia proccedings, Vol. 182. P. 3, 1990.

[4] Kren, W., Schnable, G., IEEE Transactions on Electron Devices, Vol., ED 26, No. 4, P. 647, 1979.

[5] Harbeke, G., Krausbauer, L., Steigmeier, E., RCA Reviw, Vol. 44, P. 674,1983.

[6] Reif, R., in Thin Film Process II, edited by Vossen, J., Keren, W., Academic Press, Boston, P.525,1991.

[7] Morin, F., Morel, M., Appl. Phys. Lett., Vol. 35 (9), No. 8, P. 686, 1979.

[8] Veprek, S., Iqbal, Z., Oswald, H. R., and Webb, A. P., Solid State Phys., Vol. 14, P. 295, 1981.

[9] Kamin, T., Chiang, K. L., J. Electrochem. Soc., Vol. 129, No. 10, P. 2326, 1982.

[10] Hajjar, J-J, Reif, R., Adler, D., J. Electron. Mat., Vol. 15, P. 279, 1986.

[11] Hajjar, J-J, Reif, R., J. Electrochem. Soc., Vol. 137, No. 9, P. 2888, 1990.

[12] Yamada, H., J. Vac. Sci. Technol., B7, Vol. 6 P. 1338, 1989.

[13] Luckovsky, G., Wagner, C., Nemanich, R., and Williams, M., Solar Cells, Vol. (30), P. 419, 1991.

[14] Kamin, T., Thomson, C., Polysilicon Thin Films and Interfaces, Materials Research Society Symposia, Vol. 182, 1990.

[15] Seto, J., J. Appl. Phys., Vol. 46, No. 12, P. 5247, 1975.

[16] Cowher, M. E., Sedwick, T. O., J. Electrochem. Soc., Vol. 119, P. 1565, 1972.

[17] Kamin, T., J. Appl. Phys., Vol. 42, P. 4357, 1971.

[18] Baccarani, G. Rico, B., J. Appl. Phys., Vol. 49 (11), P. 5565, 1978.

[19] Lu, C-C, Gerzberg, Chin, Lu and Meinde, L., IEEE Transactions on Electron Devices, Vol. ED-30, No. 2, P. 137, 1983.

[20] Kim, D. Khondker, A. N., Ahmed, S. S., and Shah, R., IEEE Transactions on Electron Devices, Vol. ED-31, No. 4, P. 480, 1984.

[21] Crowell, C. R., Rideout, V. L., Solid State Electronics, Vol. 12, P. 89, 1969.

[22] Sze, M. S., Physics of Semiconductor Devices, John Wiley and Sons, New York, 1981.

[23] Kraus, J., Carver, K., Electromagnetics, 2nd edition, McGraw Hill, New York 1973.

[24] Matsuda, A., J. Non-Crystalline Solids, Vol. 59&60, P. 767, 1983.

[25] Tsi, C. C, in Amorphous Silicon and Related Materials, edited by Fritzche, World Science Publication, Singapore, P. 123, 1989.

[26] Shibata, N., Fukuda, H., Ohtoshi, J., Hanna, S., and Shimizu, I., Material Research Society Symposia, Vol. 95 p. 225, 1987

[27] Dalal, V. L., Knox, R., Moradi, B., Beckle, A., and Van Zante, S., in Stability of a-Si Alloys, Materials and Devices, edited by B. Stafford, and E. Sabissky, Institute of Physics, New York, P. 249, 1987.

[28] Auciello, O., Flamm, D., Plasma Diagnostics, Vol. 1, Academic Press Inc.,

1989.

[29] Fachuet, F., Proccedings of IEEE, Vol. 80, N0. 3, P. 420, 1992.

[30] Pankove, J., Optical Properties in Semiconductors, Dove Publication Inc., New York 1971.

[31] Kohul, C., Schbtterer, H., Schwidefsky, F., J. Electrochem. Soc., Vol. 121, p.1496, 1974.

[32] Manifacier, J., Gasiot, J. and Fillard, J., J. Phys. E, Vol. 9, P. 1002, 1976.

[33] Swanepol, R., J. Phys. E., Vol. 16, P. 1213, 1983.

[34] Epstein, K., Misemer, D., Vernstrom, G., Applied Optics, Vol. 26, No. 2, P. 294, 1987.

[35] Lubberts, G., Bukery B., Moser, F. and Trabka, E. A., J. Appl. Phys., Vol. 52, No. 11, P. 6870, 1981.

[36] Iqbal, Z., Verpek, S., J. Phys. C, Solid State phys., Vol. 15, P. 377, 1982.

[37] Nakashima, S., Hagyo, M., IEEE J. Quantum Electronics, Vol. 25, P. 965, 1989.

[38] Fachuet, F., Campbell, I. H., Critical Review in Solid State and Material Sciences, Vol. 14, P. 579, 1988.

[39] Cullity, B. D., Elements of X-ray Diffraction, Addison-Wesley Reading, MA, P. 270, 1965.

[40] Azaroff, L., Elements of X-ray Crystallography, McGraw Hill, Inc., NeW York, 1968.

[41] Clug, H., Alexander, L., X-ray Diffraction Procedures for Polysilicon and Amorphous Materials, John Wiley and Sons, New York 1974.

[42] Harbeke, G., in Polycrystalline Semiconductors edited by Harbeke, G., Springer-Verlag, New York, 1985.

[43] Chiang K. L., Delloca, C. J., and Schwettmann, F. N., J. Electrochem. Soc., Vol. 126, P. 2267, 1979.

[44] Van der Pauw, L. J., Phil Tech Rev., Vol. 20, P. 220, 1958.

[45] Schroder, D. K., Semiconductor Material and Device Characterization, John Wiley and Sons Inc., New York 1990.

[46] Putley, E. H., Contem Phys., Vol. 16, P. 101, 1975.

[47] Knox, R., Dalal, V. L., Moradi, B., In Amorhous Silicon Technology, Materials Reseach Society Symposia Proceedings, edited by A. Madan, U. Hamakawa, M. J. Thompson, P. C. Taylor, and P. G. LeComber, Vol. P. PA, 1991.

[48] Dalal, V. L., Moradi, B., Baldwin, G., Amorphous Silicon Materials and Solar Cells, edited by Stafford, B., American Institute of Physics, New York, P. 298, 1991

[49] Rai-Choudhury, P., Hower, P. L., J. Electrochem Soc., Vol. 120, P. 1763, 1973.

[50] Maden, A., Shaw, M., The Physics and Applications of Amorphous Semiconductors, Academic press, Inc., Boston, 1988.

[51] Mott, N. F., Davis, E. A., Electronic Processes in Non-Crystalline Materials, Clarendon Press, Oxford, 1979.

ACKNOWLEDGEMENTS

I would like to take this opportunity to express my sincere appreciation to my major professor Dr. Vikram L. Dalal for his guidance, expertise and his willingness to help me when I needed it and let me work independently at other times.

I would also like to thank IBM Corporation for providing me the graduate fellowship. Special thank is extended to Mrs. Jane Bucshe of IBM for securing the IBM fellowship which has made the completion of my dissertation possible.

I gratefully acknowledge Dr. Ralph D. Knox for his invaluable assistance and suggestions throughout this project. This work would be never completed without his technical assistance.

I also acknowledge Dr. Stanley Burns, Dr. Howard Shanks, Dr. Scott Chumbley, Dr. Gray Tuttle and Dr. Hsung-Cheng Hsieh for serving in my committee.

Special thank is due to Dr. Douglas Robinson for the x-ray measurements and his valuable suggestions, Dr. T. Cotton and Dr. G. Chumanov of Chemistry Department for Raman spectroscopy measurements, Kay Han for metallizing some of the samples and my friend Scott DeBoer for editing the manuscript of this thesis.

I would also like to thank my friends Greg Baldwin, Sofjan Goenawan, Sanjeev Chopra, Er-Xuan Ping and Nabeeh Kandalaft who have made my stay at Iowa State University enjoyable with their friendship.

Finally, I like to express my appreciation to my wife, Tahere Fallah-Balani for her patience and encouragement throughout this project.

APPENDIX A: PAPER SUBMITTED TO J. OF ELECTRONIC MATERIALS

Properties of Polysilicon films deposited on amorphous substrates using Reactive Plasma Beam Deposition technique.

Behnam Moradi, Vikram L. Dalal and Ralph Knox*

Address: Iowa State University, Dept. of Electrical and Computer Engineering and Microelectronics Research Center, Ames, Iowa 50011
*Microelectronics Research Center, Iowa State University, Ames, Iowa 50011

Abstract

We report on the growth and properties of high mobility polycrystalline silicon films grown at low temperatures (400-500C) on amorphous substrates using a controlled reactive plasma beam deposition. The technique consists of carefully controlling the H radical flux from an electron cyclotron resonance (ECR) plasma to promote both nucleation and grain boundary passivation during growth. Using electrical and optical spectroscopy of the ECR plasma, we find that the density of H radicals impinging on the surface is one of the most important parameter controlling crystallinity of the film, and that by changing this flux, we can controllably alter the structure of the film from amorphous to polycrystalline. Unlike traditional deposition techniques for polysilicon, which requires either high deposition temperatures (650C) or a low temperature deposition followed by a post deposition anneal to achieve good mobilities, our technique produce films with mobilities of the order of 30-40 cm^2/V-sec in as grown films at considerably lower temperatures. We have produced undoped and highly doped films using this technique.

Introduction

Polycrystalline silicon (polysilicon) is an important electronic material for integrated circuits and for thin film transistors. The traditional method for depositing polycrystalline silicon is to use pyrolysis of silane in a low pressure chemical vapor deposition (LPCVD) process. In general, LPCVD polysilicon is deposited at 650-800C, a temperature that is too high for ultra large integration (ULSI). While it is possible to deposit polysilicon at lower temperatures by using precursors such as disilane, or by a plasma enhanced CVD process such as glow discharge, films deposited at lower temperatures usually have low mobilities, and need a post-deposition anneal at 700-800C to increase the mobilities [1]. In this paper, we describe a new technique which can deposit polysilicon films at low temperatures (400-500C) on amorphous substrates. These films are smooth, have grain size of about 200Å and have high electron mobilities without post-deposition annealing.

Deposition Technique

The deposition technique consists of using a reactive plasma beam of H radicals to induce growth and crystallization of the semiconductor film. We call this technique "Reactive Plasma Beam Deposition" (RPBD). The highly reactive H radicals are generated by an electron cyclotron resonance (ECR) plasma generator. The basic geometry of the apparatus is shown in figure 1 [2,3]. A microwave source generates the plasma under the influence of the magnetic field provided by the two magnets. H is introduced into the ECR chamber, and flows toward the substrate, which is located about 15 cm down stream from the resonance point of the plasma. The position of the resonance point can be

controlled by changing the relative magnitudes of the two magnetic fields. Silane is introduced near the substrate. The system is pumped by a turbo-molecular pump even during deposition to maintain high purity. Unlike previous ECR-PECVD works [4-6], we deliberately control the chemistry of growth by using a high flux of H_2 to produce H radicals which act as the primary reactive species. At these low pressures (5-20mT), the density of H is high, and thus they can travel to the substrate with little recombination. At the substrate, these H radicals combine with silane and produce silyl (SiH_3) radicals, which then lead to film growth. In addition, since H-Si bond is stronger than weak Si-Si (e.g. amorphous Si) bonds, H radicals can also be used to preferentially etch away amorphous Si during growth, leaving behind primarily crystalline Si bonds. Thus, we can promote crystallinity even at low temperatures by controlling the flux of H radicals.

These considerations are borne out by a study of the plasma chemistry. A line-of-sight optical emission spectroscopy (OES) was used to study the presence of H and H_2 species in the deposition chamber. Figure 2 shows a typical OES spectrum of the plasma near the substrate. The strong lines at 610 nm (H_2) and 656 nm (H) are particularly noteworthy. As we reduce the pressure in the reactor from 20 mT to 6 mT, both lines get stronger, since more excited radicals or molecules can travel to the substrate without losing energy. In addition, the ratio of H/H_2 lines also becomes larger, implying less recombination of H and a greater flux of H arriving at the substrate. Under these conditions (a high atomic H flux), the films produced are always polycrystalline. In contrast, when the pressure is high (20 mT), fewer H atoms are present near the substrate to

perform chemical reaction with the film, and the films are amorphous. Thus by controlling H flux, we can change the structure of the film controllably.

Structural Analysis

The crystallinity of the deposited films was examined by using the Raman spectroscopy technique. X-ray diffraction technique was used to determine the grain size and the texture of the samples. The orientation of the polysilicon films was determined by matching the 2-theta angle obtained from the x-ray diffraction with the standard value for crystalline silicon. The grain size was calculated from the line width (full width at half maximum of the x-ray spectra) by applying Scherrer formula [7].

Electrical measurements

Electronic properties of the deposited films were characterized by measuring the resistivity, Hall mobility and activation energy. We have also examined the behavior of the conductivity as a function of temperature. The resistivity, Hall mobility and carrier concentration of these films were measured using the Vander Pauw technique. All measurements were performed under dark to eliminate photovoltaics effects. Moreover, the linear current voltage relation of all contacts were examined at the range of interest prior to the measurement. This alleviates the effect of minority current injection during the measurement.

Results and Discussion

1. Deposition

The substrates used in this study were amorphous, either Corning 7059 glass or c-Si wafers with 0.4 micron thick layer of thermally grown SiO_2. For doping , we used 100 ppm PH_3, 1% PH_3, or 1% B_2H_6, all diluted in H_2. Typical flow rates were: 1 standard cubic centimeter per minute (sccm) for SiH_4 and 30-40 sccm for H_2. The doping was controlled by controlling the ratio of dopant gases to the SiH_4. The substrate temperatures used were 400-550C. Typical deposition rate were 80Å/min with a microwave power of 200W at a pressure of 6 mT. We find no influence of temperature on the deposition rate in the range studied. Similarly, the introduction of either PH_3 or B_2H_6 mixtures had no perceptible influence on the growth rate.

2. Structural Properties

Raman spectroscopy technique was applied to several undoped polysilicon films deposited at different temperatures. We have also performed Raman spectroscopy on amorphous films deposited at the same conditions as the polysilicon films but at a pressure of 15mT. Figure 3 shows the Raman spectrums of polysilicon and amorphous films deposited at 400C. The Raman spectra of the polysilicon films deposited at the higher temperatures were basically the same as figure 3. The sharp peak at 522.5 cm^{-1} indicates that the films deposited at lower pressures are indeed polysilicon, while those deposited at higher pressure (15mT) are amorphous. The asymmetry in the spectrum of polysilicon film in lower wave number is a signature of some degree of disorder in the structure. However the shoulder at about 480 cm^{-1} is much less

pronounced compared with the data in current literature [8]. This suggests that by using RPBE it is possible to grow polysilicon films with less disorder.

The results of x-ray diffraction indicate the existence of the peaks corresponding to (111), (220) and (311) planes. Other peaks were below the background level. No significant change was observed in the x ray spectra as the deposition temperature and doping rate were changed. The grain size estimated from the Scherrer's formula is 200-300Å. For the deposition parameters of this research investigation the grain size was found to be insensitive to both the dopant concentration and the type of the substrate. However a small increase in the grain size at higher temperatures was observed which may be attributed to the higher surface mobility.

3. Electrical Characteristics

The conductivity and activation energy of the intrinsic films deposited at 400C on 7059 glass substrates were 1.6×10^{-4} s/cm and 0.18 eV respectively. Higher deposition temperatures did not affect the conductivity significantly. However the activation energy increased from 0.18 to 0.21 eV as the deposition temperature increased from 400 to 550C. The introduction of PH_3 diluted in hydrogen increases the conductivity of these films by two to three orders of magnitude. We also have examined the effect of diborane on the conductivity of the polysilicon films. The conductivity of the P-type samples is lower by one order of magnitude compared to the intrinsic films. This is probably due to the compensation of the donor defects such as oxygen, and also indicate that the intrinsic films are slightly n type.

To examine the transport mechanism of polysilicon films, the conductivity of the deposited films was measured as a function of temperature. Figure 4 illustrates the result of such a measurement. At deposition pressures of 6-7 mT all the films show similar conductivity behavior in the temperature range that we investigated. However as pressure increases from 7 mT to 15 mT the conductivity decreases significantly and the behavior of the conductivity vs. temperature changes dramatically. The films deposited at 6-7mT exhibit a single activation energy, which indicate that the conduction occurs via extend states. The conductivity vs. inverse temperature of the film deposited at 15mT (a-Si) can be divided into two regions, one at high temperature and the other at low temperature. This behavior indicates the presence of two conduction mechanisms, a high activated process at high temperature and a less activated process at lower temperatures. The conduction at lower temperature has been reported to be due to the contribution of the electrons trapped in the mid gap states which hop from one localize state to another [9].

Hall mobility measurements were carried out on samples deposited on glass and silicon dioxide substrates. Highly doped ($1x10^{20}/cm^{-3}$) polysilicon films prepared on glass substrates at temperatures as low as 450C have electron mobilities as high as 40 $cm^2/V.S$. We should emphasize that such a large mobility was obtained without post deposition annealing. The Hall mobility of the lightly doped samples that we were able to measure accurately varied from 25 to 35 $cm^2/V.S$ for a doping rate of 0.6 to 3 sccm. The carrier concentration of these samples was in the range of $1x10^{16}$ to $4x10^{16}/cm^3$. These mobilites are much higher than literature data for films without post anneal ($8cm^2/V$-sec) [10].

Conclusion

We have examined the growth, structural and electrical properties of the polysilicon films deposited on amorphous substrates by reactive plasma beam deposition. The structural properties of these films show a strong dependence on the flux of incoming hydrogen radicals on the surface of the films and little dependence on the deposition temperature. The electrical characteristics of these films show high mobility as well as high conductivity without any post-anneal. Moreover, the addition of dopant gases neither suppresses the growth rate nor deteriorates the uniformity of the films.

Acknowledgements

One of us (Behnam moradi) was supported by IBM Corporation under a graduate fellowship and we thank IBM for its support. The Raman measurements were made by Dr. George Chumanov of Iowa State University, and we thank him and professor Therese Cotton for their help. This work was partially supported by a sub-contract from NREL, and used equipment donated by Polaroid Corporation.

References

[1] R. A. Ditizio, G. Liu, S. Fonash, B. Hseih and D. W. Greve, Appl. Phys. Lett. 56 (12) 1140, 1990.

[2] R. Knox, V. L. Dalal, O. A. popv, J. Vac. Sci. Tech. A9 (3) 474, (1991).

[3] R. Knox, V. L. Dalal, B. Moradi, in Amorphous Silicon Technology, 1991, edited by A. Madan, Y. Hamakawa, M. J Thomson, P. C. Taylor and P. G. Lecomber (Material Reseach Society, Pittsburg, PA, 1991).

[4] H. Yamada and Y. Torii, Appl Phys Lett. 50 (7), 386, 1986.

[5] M. Kitagawa, K. Setsune, Y. Manabe, and T. Hirao, J. Appl. Phys. 61 (5), 2084, 1987.

[6] J. J. Schellenberg, R. D. Mcleod, S. R. Mejia, H. C. Card and K. C. Kao, Appl. Phys. Lett. 48 (2), 163 1986.

[7] L. V. Azaroff, "Elements of X-Ray Crystallography," Chapter 20, McGraw-Hill Book Company, (1968).

[8] S. Vprek, Z. Iqbal, H. R. Oswald, and A. P. Webb, J. Phys. C, Solid State Phys. 14, 295 (1981).

[9] J-J. J Hajjar, R. Reif and D. Adler, J. Electron Mater., 15, 279 (1986).

[10] D. Kim, F. Quian, C. U. Bickford and S. Yu, Mat. Res. Soc. Symp. Proc., Vol. 106, 261, 1988.

Figure Captions

Figure 1. A schematic diagram of the reactive plasma beam deposition system. The reactive gas in this case is H.

Figure 2. Optical emission spectrum of the plasma near the substrate collected at 5mT and 200W.

Figure 3. Raman spectra of polysilicon and amorphous films, both deposited at 400C on glass substrates. Note the sharp peak at 522 cm^{-1} characteristrics of polysilicon film, and the broad peak at 480 cm^{-1} characteristics of the a-Si film.

Figure 4. Arhennius plot of conductivity of amorphous and polysilicon films as a function of temperature. Note the much lower activation energy for polysilicon films.

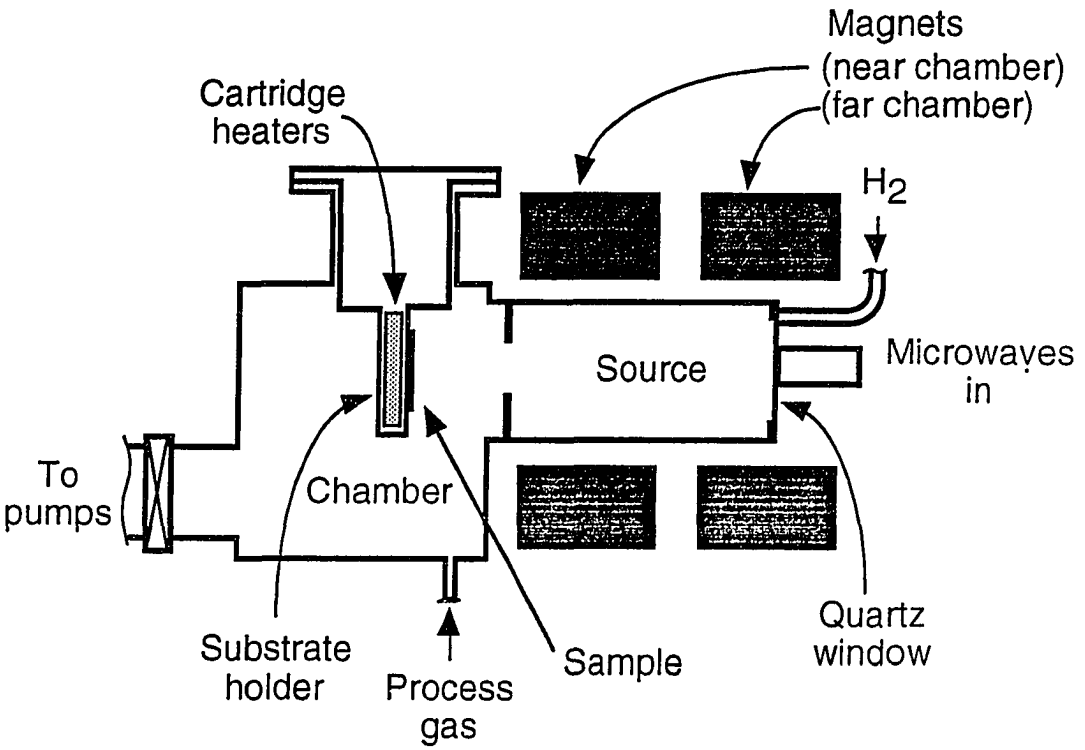
Magnets
(near chamber)
(far chamber)
Cartridge
heaters
H_2
Source
Microwaves
in
To
pumps
Chamber
Substrate
holder
Process
gas
Sample
Quartz
window

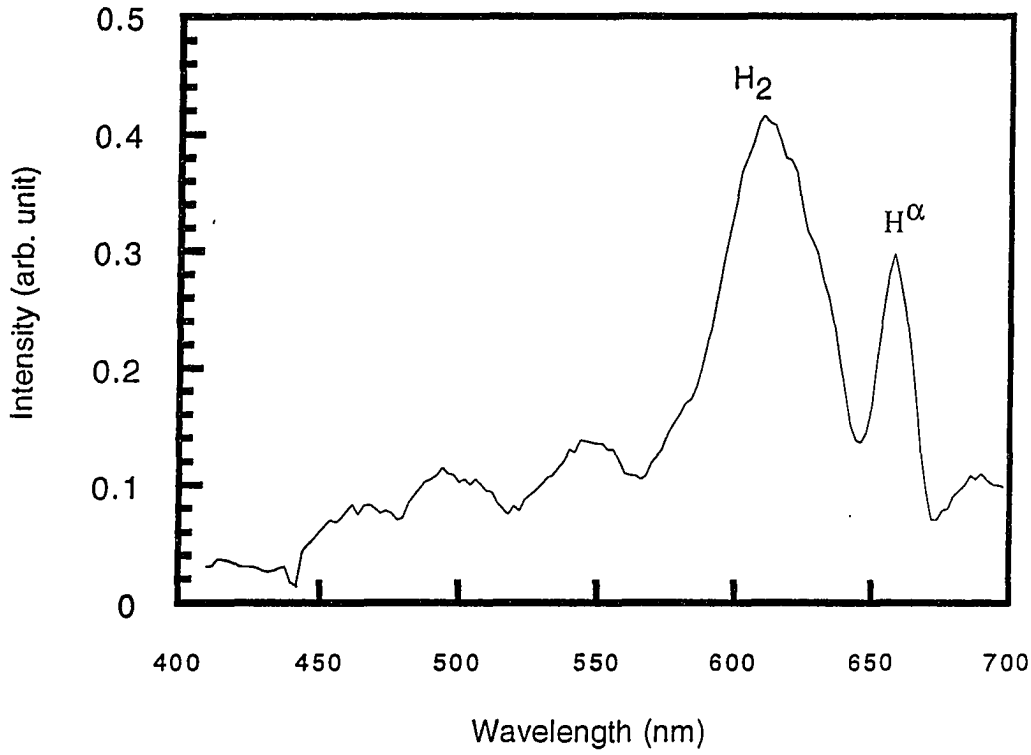
0.5
0.4
0.3
0.2
0.1
0
Intensity (arb. unit)
H_2
H^{α}
400
450
500
550
600
650
700
Wavelength (nm)

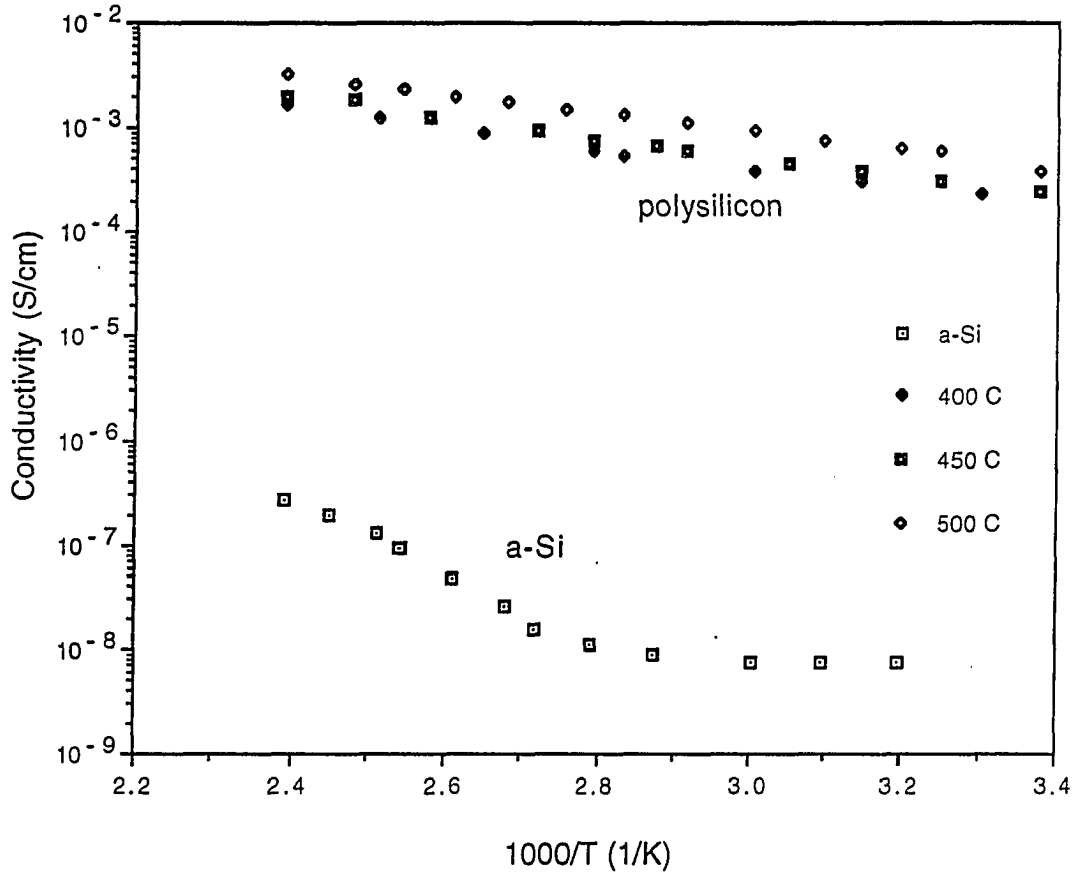
Conductivity (S/cm)
10-2
10-3
10-4
10-5
10-6
10-7
10-8
10-9
2.2
2.4
2.6
2.8
3.0
3.2
3.4
1000/T (1/K)
polysilicon
a-Si
a-Si
400 C
450 C
500 C

APPENDIX B: SIMS ANALYTICAL CONDITIONS

Following is the SIMS analytical conditions used by the Charles Evans & Associates for the depth profile of the samples discussed in the text.

In a typical SIMS analysis, the samples are sputtered by a focused energetic primary ion beam (of current I_p) which is rastered over a square area, usually a few hundred microns on a side. Secondary ions formed during the sputtering process are accelerated away from the sample surface by a nominal sample voltage of 4500V. A fraction of the secondary ions are accepted for the analysis by the secondary mass spectrometer and are collected from circular image area centered in the rastered region. This field of view is defined by an adjustable field aperture (FA) in the ion optic column. This aperture provides an optical gate that is used to improve depth resolution by rejecting secondary ions emitted from the wall of the sputtered crater where material at different depths is exposed simultaneously. The transmission (sensitivity) of the secondary spectrometer is further controlled by a second adjustable aperture (contrast diaphragm, CD) in the secondary ion optic column. Adjustable entrance and exit silts are used to adjust the mass resolution of the spectrometer when it is necessary to separate interfering ions of the same nominal mass/charge ratio. The secondary ions are energy focused by a spherical electrostatic analyzer, and mass/filtered by a magnetic sector analyzer. After passing through the analyzers, the ions are detected either in an analog current mode using a faraday cup, or in a pulse counting mode typically using an electron multiplier.

Cs SIMS Analytical Conditions

Beam Species	Impact energy	Secondary polarity	FC/EM ratio	Image field um
CS^+	14.5eV	positive	1.18	150

Element	FA (um)	CD (um)	Ip (uA)	Raster (um)	Sputter Rate (Å/S)
H, C, O	30	25	0.5	500	14
P(HRM)	30	150	0.5	350	33

SIMS profile of a float zone crystalline silicon

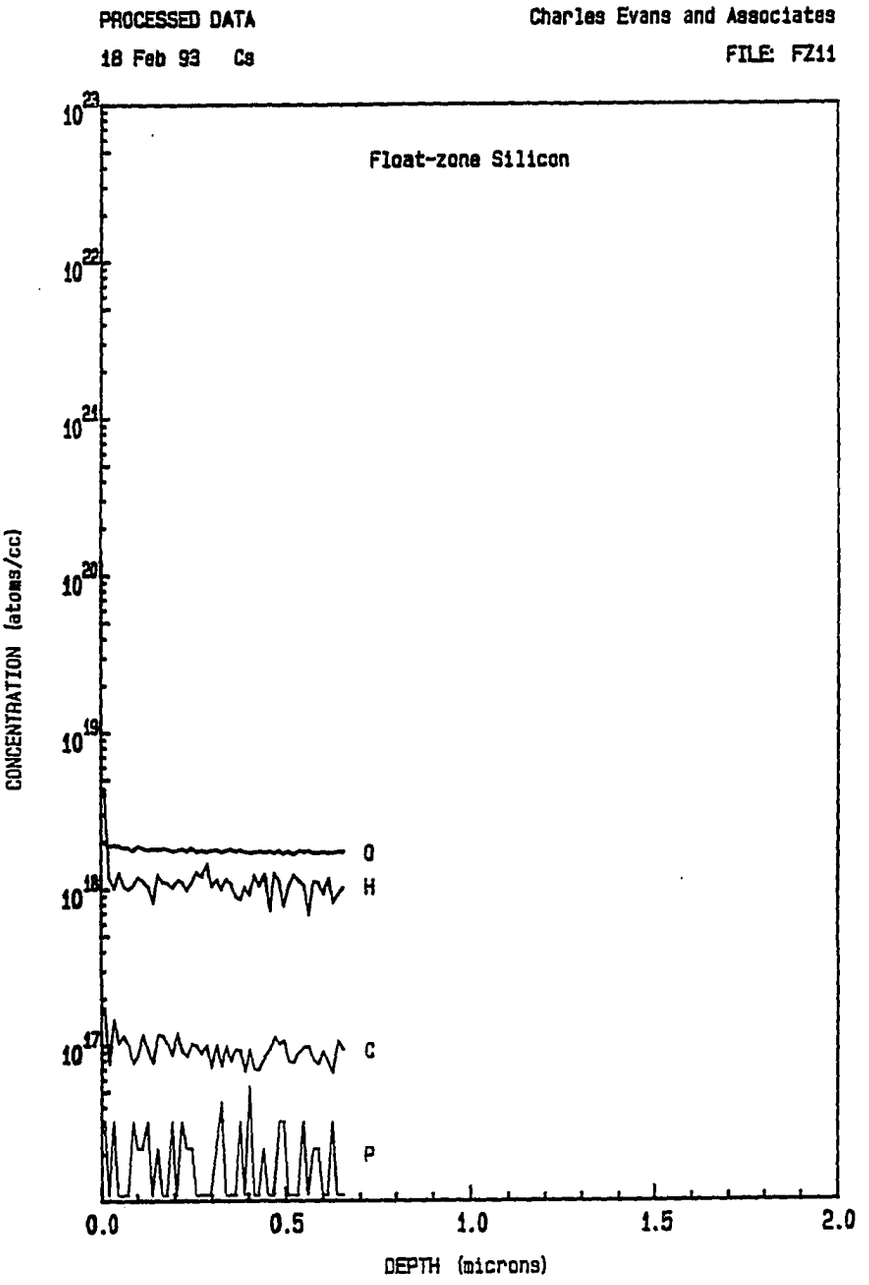

APPENDIX C: RAMAN SPECTRA OF SILICON, POLYSILICON AND AMORPHOUS SILICON